ANL-6669

Argonne National Laboratory

CRITICAL STUDIES OF CORE B FOR THE ENRICO FERMI ATOMIC POWER PLANT (ZPR-III Assembly No. 35)

by

T. A. Doyle and A. L. Hess

ANL-6669
Reactor Technology
(TID-4500, 19th Ed.)
AEC Research and
Development Report

ARGONNE NATIONAL LABORATORY
9700 South Cass Avenue
Argonne, Illinois

CRITICAL STUDIES OF CORE B FOR THE ENRICO FERMI ATOMIC POWER PLANT (ZPR-III Assembly No. 35)

by

T. A. Doyle* and A. L. Hess

Idaho Division

*On loan to Idaho Division from Atomic Power Development Associates, Inc., for this experiment.

February 1963

Operated by The University of Chicago
under
Contract W-31-109-eng-38
with the
U. S. Atomic Energy Commission

TABLE OF CONTENTS

	Page
ABSTRACT	11
INTRODUCTION	11
I. DESCRIPTION OF FERMI CORE B	12
II. DESCRIPTION OF ASSEMBLY	15
III. THE CRITICAL EXPERIMENT PROGRAM	21
IV. THE CRITICAL EXPERIMENT	23
A. Critical Experiment without Nickel Reflector	23
1. Approach to Critical	23
2. Control-rod Calibration	25
3. Measurements of Edge Worth and Critical Mass	25
B. Critical Experiment with Nickel Reflector	26
1. Approach to Critical	26
2. Control-rod Calibration	28
3. Measurements of Reflector Worth and Critical Reflector	28
V. ENGINEERING FEATURES OF FERMI CORE B	30
A. Reactivity Effect of End Gaps	30
B. Reactivity Effect of UO_2 Axial Blankets	31
1. Worth of Axial Nickel Reflectors	35
2. Reactivity Effect of Streaming Paths	35
C. Reactivity Effect of Central Gap	35
D. Antimony-Beryllium Source	37
VI. KINETICS FEATURES	39
A. Isothermal Temperature Coefficient	39
B. Reactivity Effect of Axial Core Expansion	39
C. Measurement of Rossi-Alpha	39

TABLE OF CONTENTS

		Page
VII.	SAFETY AND CONTROL CHANNELS AND RODS; OSCILLATOR ROD	40
	A. Reactivity Worths of Safety and Control Channels	40
	B. Reactivity Worth of Safety Rod	42
	C. Reactivity Worth and Variation of Oscillator Rod	43
	D. Reactivity Worth of Control Rod	45
VIII.	HETEROGENEITY EFFECT OF FUEL	47
IX.	REACTIVITY COEFFICIENTS	50
	A. Distributed Reactivity Worths	50
	B. Radial Worths of Enriched Uranium and Sodium Columns	51
	C. Local Reactivity Worths of Sodium	54
	D. Variation of Sodium Reactivity Coefficient with Sodium Density	56
	E. Local Reactivity Worths	58
	F. Radial and Axial Traverses of Fissionable Materials	60
	1. Traverses along Core Axis	60
	2. Traverses at Core Radial Edge Parallel to Axis	60
	3. Radial Traverses at Midplane with Nickel Reflector	62
	4. Radial Traverses at Midplane with Type "B" Nickel Oxide Reflector	63
X.	COMPARISON OF REFLECTOR WORTHS	64
	A. Reactivity Effects of Types "A" and "B" Nickel-reflector Thicknesses	64
	B. Reactivity Effects of Various Reflectors	66
XI.	THE CRITICAL TYPE "B" NiO REFLECTOR	71
XII.	REACTION RATE TRAVERSES	75
	A. Traverses along Assembly Axis	76

TABLE OF CONTENTS

		Page
	B. Traverses at Core Radial Edge Parallel to Axis	77
	C. Radial Traverse at Midplane with Type "A" Nickel Reflector	79
	D. Radial Traverse at Midplane with Type "B" NiO Reflectors	80
XIII.	FOIL IRRADIATIONS	82
	A. Foil Irradiations at Midplane with Nickel Reflector	82
	B. Foil Irradiations at Midplane with Nickel Oxide Reflector	83
XIV.	CENTRAL FISSION RATIOS	83
REFERENCES		87
APPENDIX A - ZPR-III, Assembly 35 Specifications		89
APPENDIX B - Derivation of Inhour Curve		90
APPENDIX C - Measurement of Reactor Subcriticality with BF_3 Neutron Counters in ZPR-III		92
ACKNOWLEDGEMENTS		95

LIST OF FIGURES

No.	Title	Page
1.	Perspective View of Fermi Reactor	13
2.	Horizontal Cross Section of Fermi Reactor	14
3.	Vertical Cross Section of Core B	15
4.	View of ZPR-III Critical Facility Showing Fermi B Mockup	16
5.	Typical Core and Axial Blanket Drawers	16
6.	Core and Axial Fine Blanket Drawer, Type 1	17
7.	Core and Axial Fine Blanket Drawer, Type 2	17
8.	Core and Axial Fine Blanket Drawer, Type 3	17
9.	Core and Axial Fine Blanket Drawer, Type 4	18
10.	Core and Axial Fine Blanket Drawer, Type 5	18
11.	Core and Axial Fine Blanket Drawer, Type 6	18
12.	Core and Axial Fine Blanket Drawer, Type 7	19
13.	Core and Axial Fine Blanket Drawer, Type 8	19
14.	Radial Fine Blanket Drawer, Type 1	20
15.	Radial Fine Blanket Drawer, Type 2	20
16.	Interface View of Assembly with Planned 587-liter Core	21
17.	Horizontal Section through Assembly at Drawer Row P	21
18.	Approach to Criticality without Nickel Reflector; Inverse Power Versus U^{235} Loading	24
19.	Approach to Criticality without Nickel Reflector; Inverse Power x U^{235} Loading Versus U^{235} Loading	24
20.	Interface View of Assembly with 667-liter Core	24
21.	Calibration of Control Rod No. 10 in 667-liter Core	25
22.	Assembly with 599-liter Core and Critical Type "A" Nickel Radial Reflector	26
23.	Nickel-reflector Drawer, Type "A"	27
24.	Approach to Criticality with 599-liter Core by Addition of Type "A" Nickel Reflector	27
25.	Calibration of Control Rod No. 10 ("Seeded") in 599-liter Core with Nickel Reflector	28

LIST OF FIGURES

No.	Title	Page
26.	Assembly Configuration for End Gap and UO_2 Axial Blanket Experiments	30
27.	Upper UO_2 Axial Blanket Drawer, High Density	31
28.	Lower UO_2 Axial Blanket Drawer, High Density. (Represents two of a three-drawer sequence)	32
29.	Lower UO_2 Axial Blanket Drawer, High Density. (Represents one of a three-drawer sequence)	32
30.	Assembly Configuration for Center Gap Experiment	36
31.	Half No. 1 Drawer Loadings of Beryllium-source Mockup	37
32.	Fission Rates of Enriched Uranium at Midplane in Beryllium-source Experiment	38
33.	Assembly Configuration for Rossi-Alpha Measurements	40
34.	Assembly Configuration for Reactivity Worths of Control and Safety Rods and Channels	41
35.	Cross Secthion through Safety-rod Mockup	43
36.	Cross Section through Oscillator-rod Mockup	44
37.	Reactivity Response of Oscillator-rod Rotation	45
38.	Cross Section through Control-rod Mockups	46
39.	Assembly Configuration for Fuel Heterogeneity Experiments	48
40.	Drawer Arrangements for Fuel-bunching Experiment	48
41.	Drawer Arrangement for Fuel-unbunching Experiment	49
42.	Results of Fuel Heterogeneity Experiments Applied to Entire Core	49
43.	Assembly Configuration for Distributed Worths Experiments	51
44.	Assembly Configuration for Measurements of Worth of Enriched Uranium Column	52
45.	Reactivity Worth of Enriched Uranium Column Versus Radius	53
46.	Assembly Configuration for Measurements of Worth of Sodium Column	53
47.	Reactivity Worth of Sodium Columns Versus Radius	54

LIST OF FIGURES

No.	Title	Page
48.	Assembly Configuration for Measurements of Local Sodium Worth	55
49.	Reactivity Worth of Sodium in Local Volumes	56
50.	Outline of Core Zones for Sodium Density-Worth Experiments	56
51.	Assembly Configuration for Local Reactivity Worth Measurements	58
52.	Axial Traverses of 93.1% Enriched Uranium Sample at Radii = 0 and 17.4 in.	61
53.	Axial Traverse of Natural Uranium Sample at Radius = 0 in.	61
54.	Radial Traverses of 93.1% Enriched Uranium Sample at Midplane through Ni and NiO Reflectors	63
55.	Radial Traverse of Natural Uranium Sample at Midplane through Ni and NiO Reflectors	63
56.	Outline of Radial Zones for Nickel-reflector Thickness-Worth Measurements	65
57.	Reactivity Worth Versus Thickness of Nickel-reflectors Types "A" and "B"	66
58.	Assembly Configuration for Experiments with Radial Reflectors of Different Compositions	67
59.	Drawer Loading for ZPR-III Type "A" NiO Reflector	68
60.	Drawer Loading for ZPR-III Fe_2O_3 Reflector	69
61.	Drawer Loading for ZPR-III Be Reflector	69
62.	Drawer Loading for ZPR-III BeO Reflector	70
63.	Nickel Oxide Reflector Drawer, Type "B"	72
64.	Interface View of Assembly with 599-liter Core and Critical Type "B" Nickel-Oxide Reflector	73
65.	Axial Traverses of Enriched Uranium and Depleted Uranium Fission Counters in 1- and 2-P-16 (Radius = 0 in.)	77
66.	Axial Traverses of $B^{10}F_3$ and Pu^{239} Counters in 1- and 2-P-16 (Radius = 0 in.)	77
67.	Axial Traverses of Enriched Uranium and Depleted Uranium Fission Counters in 1- and 2-H-16 (Radius = 17.4 in.)	78

LIST OF FIGURES

No.	Title	Page
68.	Axial Traverses of $B^{10}F_3$ and Pu^{239} Counters in 1- and 2-H-16 (Radius = 17.4 in.).	78
69.	Enriched Uranium Fission Rate Versus Radius at Midplane through Nickel and Nickel Oxide Reflectors.	80
70.	Depleted Uranium Fission Rate Versus Radius at Midplane through Nickel and Nickel Oxide Reflectors.	80
71.	Radial Traverse of $B^{10}F_3$ Counter at Midplane through Nickel Reflector.	80
72.	Absolute Fission Chambers	84
73.	Inhour Curve for Assembly 35 with 599-liter Core and Type "A" Nickel Reflector	91

LIST OF TABLES

No.	Title	Page
I.	Regional Compositions (v/o) and Densities (g/cc) of Fermi Core B	11
II.	Regional Compositions (g/cc) of Initial Critical Assembly	22
III.	Main Dimensions of Critical Assembly	25
IV.	Regional Compositions (g/cc) of Core, Fine Blankets, and Nickel Reflector in Nickel-reflected Assembly (599-liter Core)	27
V.	Results of UO_2 Axial Blanket Experiments	33&34
VI.	Beryllium-source Experiment: Composition Changes in "Source Channel"	37
VII.	Radiochemical Analysis of Foils Irradiated for Beryllium-source Experiment	38
VIII.	Compositions (g/cc) for the Safety and Control-channel Experiments	42
IX.	Reactivity Worth and Variation of the Oscillator-rod Mockup	44
X.	Compositions and Reactivity Worths of Various Control-rod Mockups	47
XI.	Distributed Reactivity Worths	50
XII.	Worth of Enriched Uranium Column at Various Radii	52
XIII.	Worths of Sodium Columns at Various Radii	54
XIV.	Local Reactivity Worths of Sodium	55
XV.	Effect of Sodium Density on Its Reactivity Worth	57
XVI.	Local Reactivity Worths of Materials	59
XVII.	Axial Traverses of Uranium Reactivity Samples	61
XVIII.	Radial Traverses of Uranium Reactivity Samples at Assembly Midplane	62
XIX.	Nickel-reflector Worth as a Function of Composition and Thickness	65
XX.	Compositions of Possible Fermi Reflectors and Their Mockups	67
XXI.	Material Worths in the ZPR-III Reflectors	68

LIST OF TABLES

No.	Title	Page
XXII.	Comparison of Worths of Various Reflectors in One Quadrant of One Assembly Half	71
XXIII.	Comparison of Enriched Uranium Column Worths with Ni and NiO Reflectors	74
XXIV.	Comparison of Sodium Column Worths with Ni and NiO Reflectors	74
XXV.	Specifications of Fission and $B^{10}F_3$ Traverse Counters	75
XXVI.	Axial Counter Traverses through 1- and 2-P-16 (Radius = 0 in.)	76
XXVII.	Axial Traverses of Counters through 1- and 2-H-16 (Radius = 17.4 in.)	78
XXVIII.	Radial Fission Rate Traverses at Core Midplane with Nickel Reflector	79
XXIX.	Radial Traverse of BF_3 Counter at Core Midplane with Nickel Reflector	79
XXX.	Radial Fission Rate Traverses at Core Midplane with NiO Reflector	81
XXXI.	Foil Irradiations at Midplane with Nickel Reflector	82
XXXII.	Foil Irradiations at Midplane with Nickel Oxide Reflector	83
XXXIII.	Central Fission Ratio Measurements with Absolute Counters	85

CRITICAL STUDIES OF CORE B FOR THE ENRICO FERMI ATOMIC POWER PLANT (ZPR-III Assembly No. 35)

by

T. A. Doyle and A. L. Hess

ABSTRACT

This report is concerned with the critical studies of a simplified mockup of the second loading (Core B) for the Enrico Fermi fast reactor. The core consists of a fully enriched, UO_2-stainless steel cermet clad in stainless steel and cooled by sodium. The high critical mass found for the reactor mockup led to a series of experiments on reducing neutron leakage from the core by surrounding it with different reflectors. With a nickel reflector in place, measurements were made of the reactivity worths of various engineering features of the Fermi reactor, distributed and local reactivity coefficients, various fission and capture rates and fission ratios, and the prompt-neutron lifetime. Finally, with a nickel oxide reflector in place, some of the above measurements were repeated.

INTRODUCTION

The composition of Core B of the Enrico Fermi fast reactor is 11.5 v/o fully enriched UO_2, 51.8 v/o stainless steel, and 33.2 v/o sodium (see Table I) in a nominal maximum volume of 600 liters. No critical experiments had yet been performed which resemble Core B in size or spectrum when this work was undertaken. An underestimation of reactivity could have serious consequences since the available core volume allows little flexibility. Hence, the need for a critical experiment was established.

Table I

REGIONAL COMPOSITIONS (v/o) AND DENSITIES (g/cc) OF FERMI CORE B

Material	Core	Safety Rod Channel	Control Rod Channel	End Gaps		Axial Blanket		Radial Blanket	Safety Rod (1)	Control Rod (1)
				Upper	Lower	Upper	Lower			
				Volume Percent						
UO_2 (93% enriched)	11.54					31.1	19.9			
UO_2 (depleted)						19.6	17.4	18.6	16.0	20.0
Stainless Steel	51.81	20.0	20.0	32.3	33.7	45.1	60.0	39.1	63.0	66.6
Sodium	33.23	80.0	80.0	67.7	66.3			42.3		
Depleted U-2.75 w/o Mo									9.8*	11.0*
B_4C						4.2	2.7		11.2	2.4
Void	3.42									
				Regional Density (g/cc)						
UO_2 (93% enriched)	1.26					3.409	2.181			
UO_2 (depleted)						1.55	1.37	1.47	1.26	1.58
Stainless Steel	4.10	1.58	1.58	2.55	2.66	0.39	0.57	0.34	0.54	0.57
Sodium	0.29	0.69	0.69	0.58	0.57			7.72		
Depleted U-2.75 w/o Mo									0.24	0.27
B_4C										

*Assumes density B_4C = 2.42 g/cc.

To make the results of the experiment of general application, it was decided to perform it on a simplified mockup of the actual reactor. A uniform core, in which the safety and control-rod channel compositions were averaged into the core, surrounded by a uniform blanket, would be taken as the basic assembly, omitting the various engineering features of the Fermi reactor, such as end gaps described in Section I below. The reactivity effects of these and other Core B details would be determined in separate experiments.

The experiment was carried out under the terms of a contract between the Atomic Energy Commission and Power Reactor Development Company, covering development work on the Enrico Fermi reactor [AEC Contract AT(11-1)-476]. The Zero Power Reactor III (ZPR-III), a fast critical facility of Argonne National Laboratory at the National Reactor Testing Station in Idaho, was used for the experiments. The experimental program for the mockup, known as ZPR-III Assembly 35, was carried out between August 1961 and February 1962. A similar experiment was performed on a mockup of Core A for the Enrico Fermi reactor and is reported in ANL-6629.(1)

I. DESCRIPTION OF FERMI CORE B

A general description of the Enrico Fermi plant is given in APDA-124.(2) The Core B subassemblies are designed for this plant, with the pump capacity and the limitation on the number of core subassemblies as the two major factors to be considered. Core B subassemblies have the same overall dimensions as those of Core A, the only significant difference being in the core and blanket sections of these subassemblies. A perspective view of the Fermi reactor is given in Fig. 1.

The Core B fuel, a dispersion of UO_2 in stainless steel, is in the form of plates 19 x 2.312 x 0.115 in.; these dimensions include the stainless steel cladding. Each plate contains initially 158 g of U^{235} in the form of fully enriched uranium. Fourteen of these plates are arranged in a bundle with a coolant passage of 54 mils between adjacent plates. Two fuel-element bundles, assembled one above the other, comprise the core section in the subassembly can. Immediately above and below the core section are end gaps, which allow for flow redistribution and contain structural support for fuel plates and blanket pins. The end gaps are slightly over 3 in. high. The axial blanket pins contain depleted UO_2 of 90% density. The pins are 13 in. long and 0.391 in. in OD, including the stainless steel cladding. The upper axial blanket contains 25 pins in a uniform arrangement. In the lower blanket, the central nine pins are omitted to provide an open channel in the event of meltdown. The radial blanket design is the same as for Core A and consists of a depleted uranium-molybdenum alloy.(2)

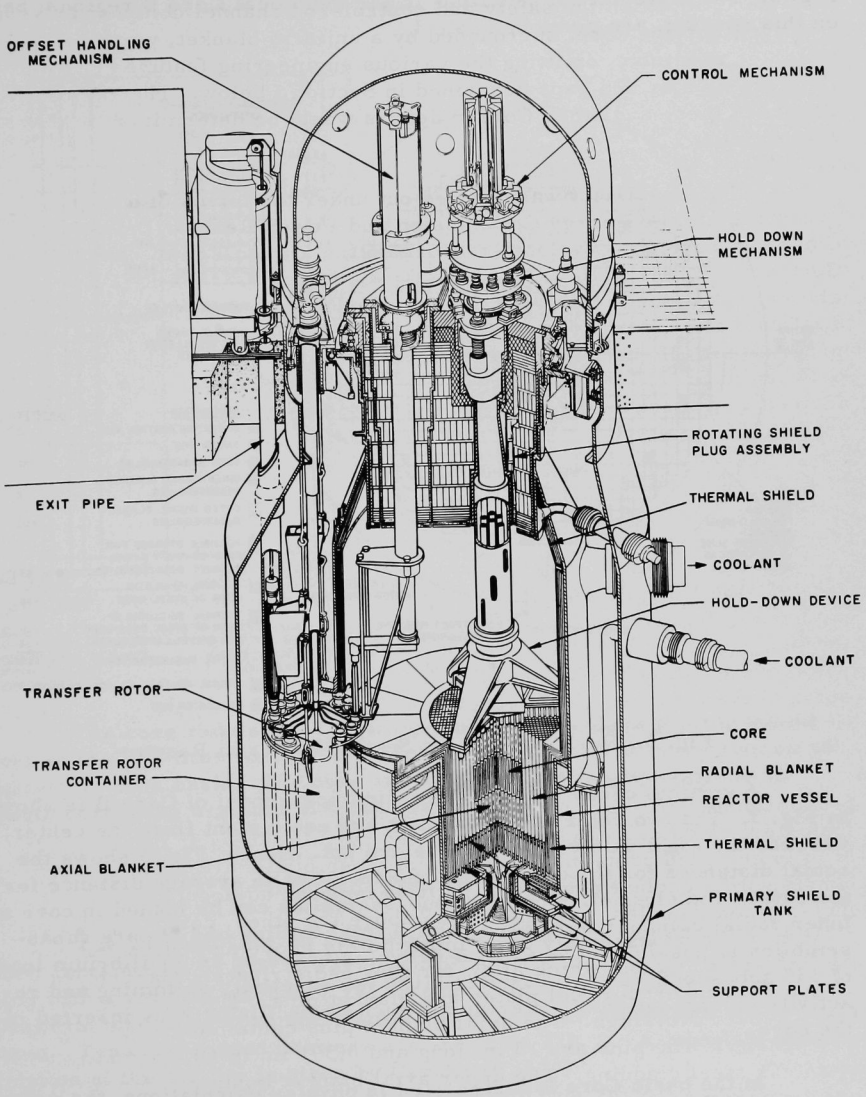

Fig. 1. Perspective View of Fermi Reactor

The core and axial blanket, and radial blanket materials are arranged in square stainless steel cans on a matrix spacing of 2.693 in., as shown in Fig. 2. The material compositions of the individual Core B regions, based on this spacing, are given in Table I.

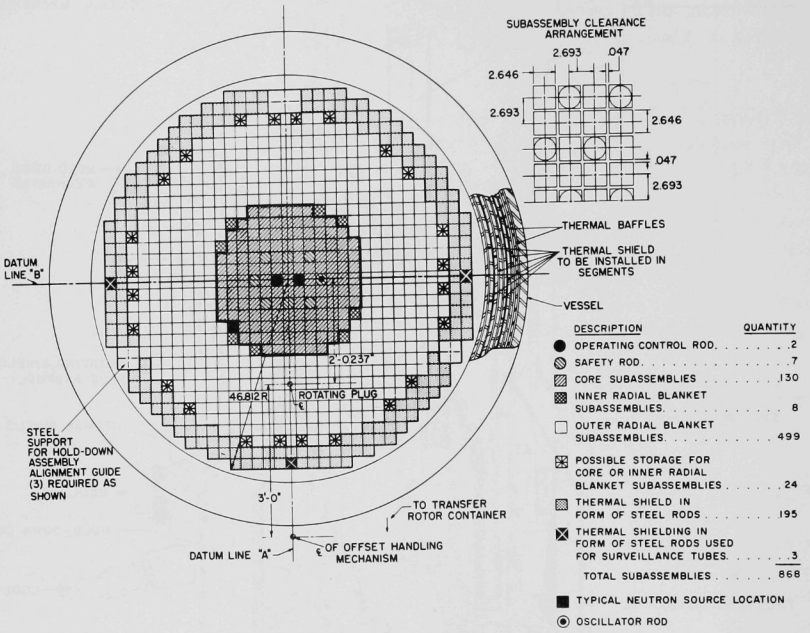

Fig. 2. Horizontal Cross Section of Fermi Reactor

A vertical cross section of a cylindrical model of Core B is shown in Fig. 3. The two control rod channels are equidistant from the center, whereas the eight safety rod channels are not. Hence, Fig. 3 shows the actual distances for the control-rod channel, but an average distance for the safety-rod channel. Core fuel subassemblies can be loaded in core and inner radial blanket positions, so that a total loading of 139 core subassemblies is possible. The Core B design is based on an equilibrium loading of 130 subassemblies to allow flexibility for reactivity shimming and reactivity compensation of experiments such as oscillator rods inserted in the core.

In the basic Core B design used in physics calculations, the central gap, "F" in Fig. 3, has been omitted, and the core section regarded as continuous 36-in. fuel plates. The 130 subassemblies along with the 10 control and safety-rod subassemblies shown on Fig. 2 would then occupy a core

volume of 600 liters. In the event of a reactivity underestimate, it was proposed to use nickel reflector subassemblies around this core, i.e., replacing radial blanket, for additional reactivity.

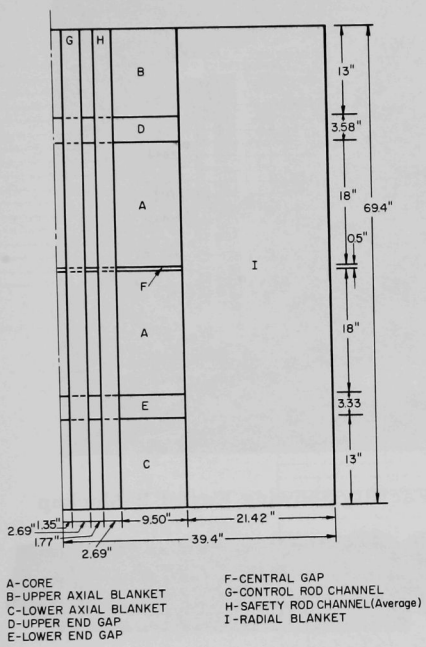

Fig. 3

Vertical Cross Section of Core B

The core radius of 17.98 in. given in Fig. 3 is for the equivalent area of the 600-liter core. The radius of the radial blanket is also on an equivalent area basis. The core and axial blanket lengths refer to the length containing uranium in these regions.

II. DESCRIPTION OF ASSEMBLY

The ZPR-III (Fig. 4) consists of one fixed and one movable half, each containing a 31 x 31 array of horizontal stainless steel tubes, 33.5 in. long with a vertical pitch of 2.176 in. and a horizontal pitch of 2.184 in. Drawers containing core and blanket materials are loaded into these matrix tubes. Typically loaded drawers are shown on Fig. 5. A complete description of the facility is given by Cerutti et al.(3)

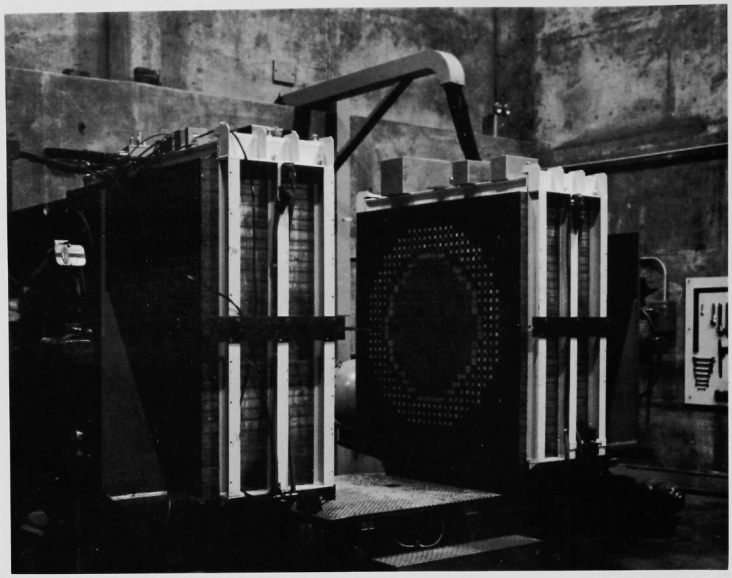

Fig. 4. View of ZPR-III Critical Facility Showing Fermi B Mockup

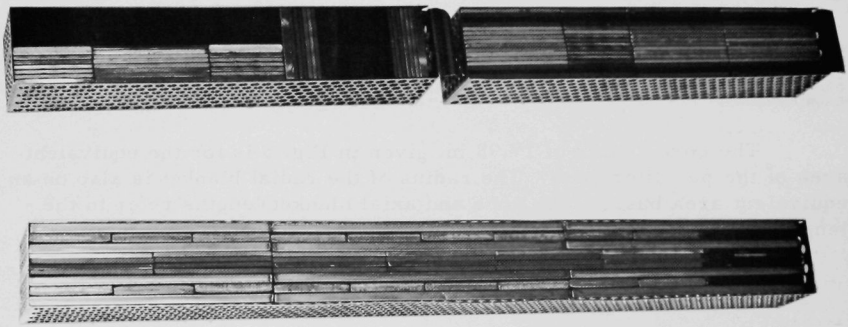

Fig. 5. Typical Core and Axial Blanket Drawers

The type and size of materials available in the experiment mainly determine the accuracy of the composition mockup. For the first time in a large core experiment, sodium was available in sufficient quantity to allow its use in the core and inner blanket regions. It was necessary, however, to mock up the UO_2 by means of fully enriched uranium and iron oxide (Fe_2O_3) pieces. These materials were arranged in a unit module, consisting of a sufficient number of drawers to allow close representation of the Fermi core composition. This unit module was then repeated

throughout the core. In this core it was necessary to use an eight-drawer sequence as the unit module. A top view of these eight drawers is shown in Figs. 6-13. Their average composition represents that of a homogeneous core, i.e., the active core with the control and safety-rod channels.

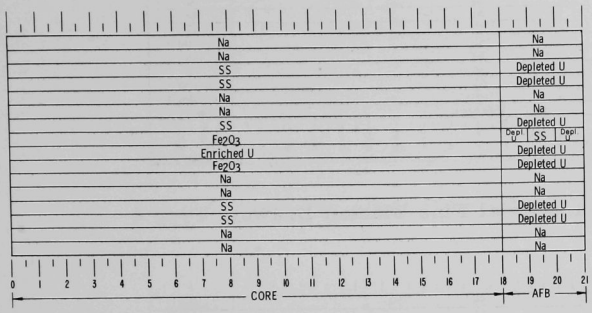

Fig. 6

Core and Axial Fine Blanket Drawer, Type 1

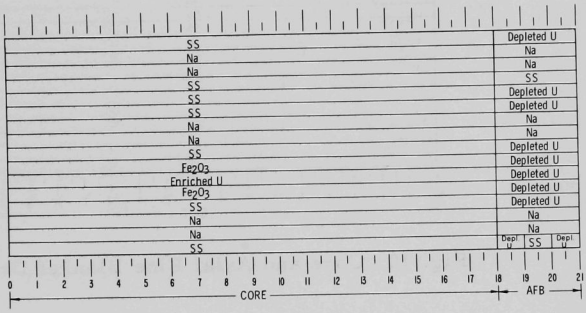

Fig. 7

Core and Axial Fine Blanket Drawer, Type 2

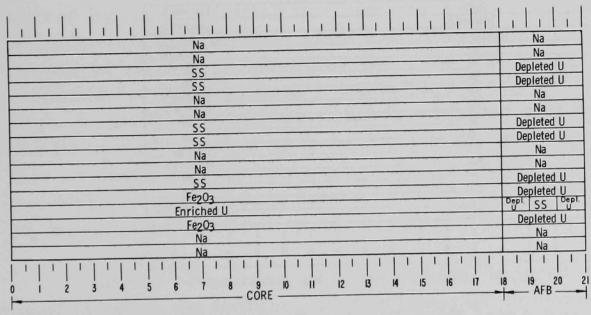

Fig. 8

Core and Axial Fine Blanket Drawer, Type 3

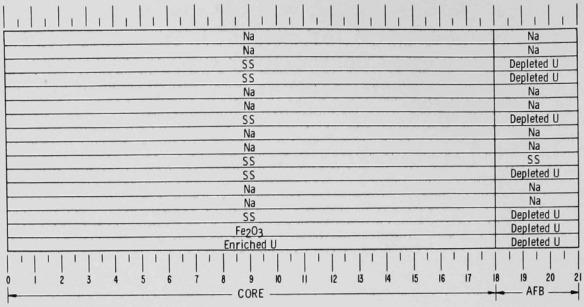

Fig. 9. Core and Axial Fine Blanket Drawer, Type 4

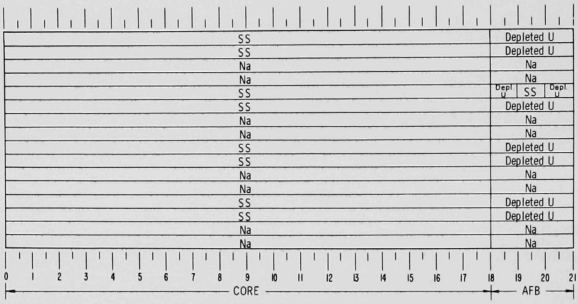

Fig. 10. Core and Axial Fine Blanket Drawer, Type 5

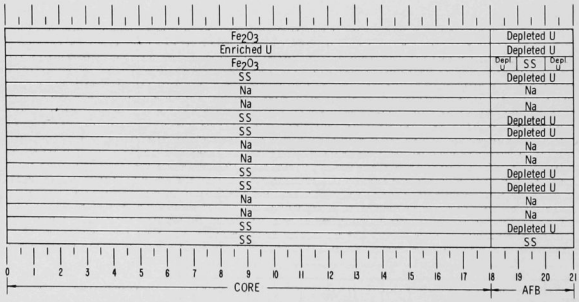

Fig. 11. Core and Axial Fine Blanket Drawer, Type 6

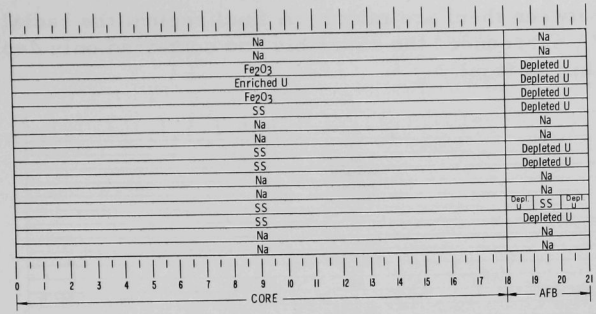

Fig. 12. Core and Axial Fine Blanket Drawer, Type 7

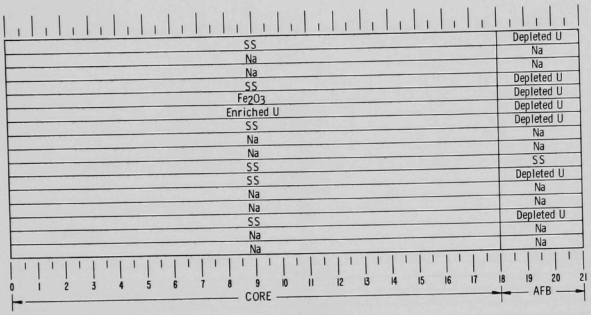

Fig. 13. Core and Axial Fine Blanket Drawer, Type 8

An entirely uniform mockup of the radial and axial blankets, as required by the simplified mockup conception, was not fully achieved because of materials limitations. The use of sodium was continued in the first few inches of blanket surrounding the core. In the axial direction this blanket extended for 3 in. on both sides behind the core and is also shown in Figs. 6-13; it is known as axial fine blanket (AFB). The radial fine blanket (RFB) was also intended to be 3 in. wide, but the final use of a reflector in this position modified this blanket. The RFB was initially mocked up in a two-drawer unit module known as RFB No. 1 and 2, shown on Figs. 14 and 15, respectively.

In the remaining axial and radial blanket regions, aluminum was used to mock up sodium. On the basis of previous ZPR-III experiments, it was decided to use an equivalence of 1.21 atoms aluminum to each sodium atom. There were four such regions: two axial medium blankets (AMB No. 1 and 2), and two radial medium blankets (RMB No. 1 and 2). The composition

differences between them are minor. A final region, the radial coarse blanket (RCB), surrounded the assembly and contained only depleted uranium and stainless steel.

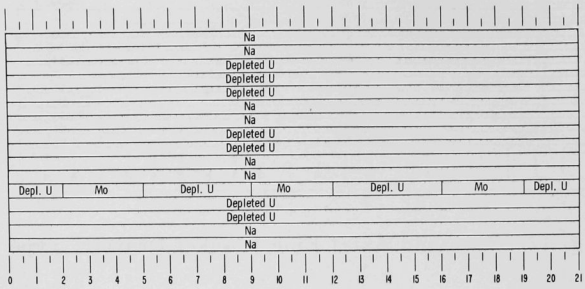

Fig. 14. Radial Fine Blanket Drawer, Type 1

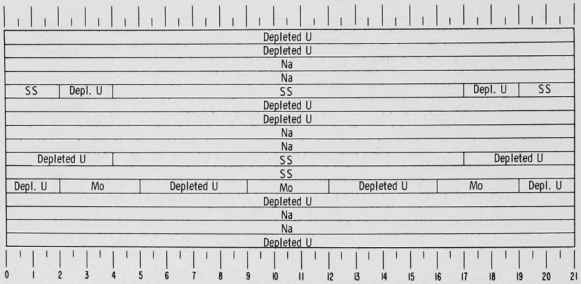

Fig. 15. Radial Fine Blanket Drawer, Type 2

The assembly as originally planned with these various regions is shown on Figs. 16 and 17. This planned core size was too small for criticality, however, so that alterations in the core, AFB, and RFB radial dimensions were necessary. All other regions remained as shown on Figs. 16 and 17 throughout all experiments. The compositions of these latter regions are given in Table II; the core and fine blanket compositions in this table refer to the critical assembly without nickel reflector (the precise core and fine blanket compositions vary with core size because of the edge patterns).

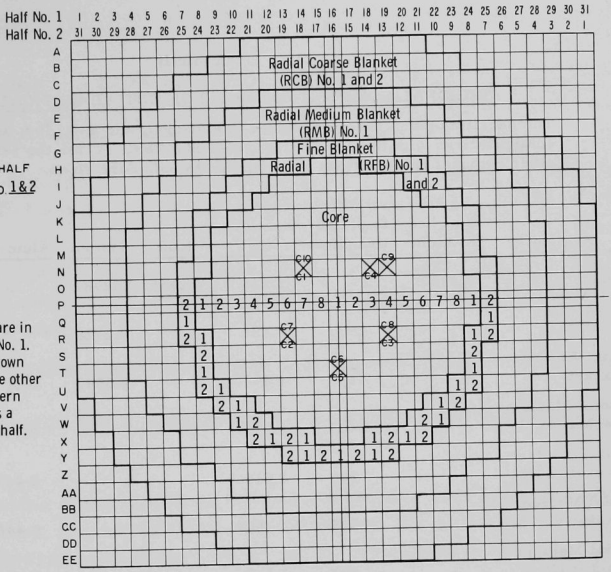

Note: Control/safety rods C1-C5 are in Half No. 2, C6-C10 in Half No. 1. The core drawer pattern shown for row P is identical in the other rows. The RFB drawer pattern shown for the lower half is a mirror image of the upper half.

Fig. 16. Interface View of Assembly with Planned 587-liter Core

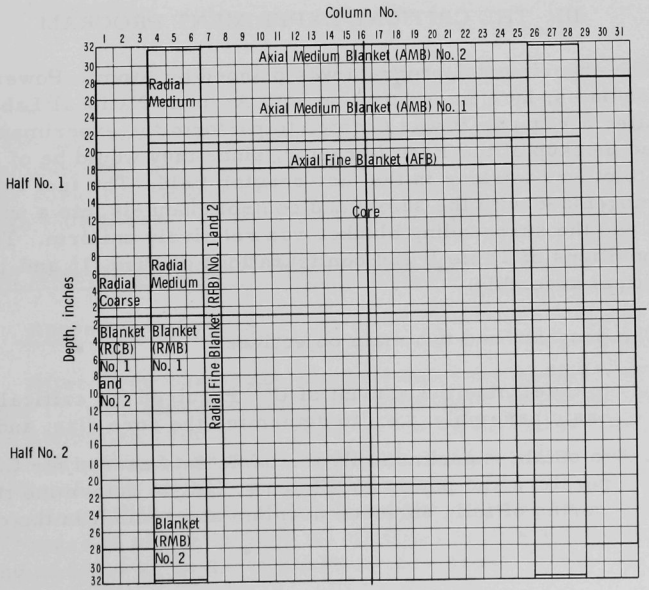

Fig. 17. Horizontal Section through Assembly at Drawer Row P

Table II

REGIONAL COMPOSITIONS (g/cc) OF INITIAL CRITICAL ASSEMBLY

The densities given for core, radial fine blanket, and axial fine blanket refer to their configurations with the 666.7-liter core. See Table IV for the 599.3-liter core. All other regional compositions are common to both core sizes.

Region	93.2% Enriched Uranium	0.21% Depleted Uranium	Stainless Steel	Iron	Sodium	Aluminum	Oxygen	Molybdenum
Core	0.8160	-	3.628	0.2655	0.2987	-	0.1058	-
Radial Fine Blanket	-	7.531	1.481	-	0.2728	-	-	0.2223
Axial Fine Blanket	-	7.539	1.499	-	0.3040	0.0037	-	-
Radial Medium Blanket No. 1	-	7.486	1.511	-	-	0.4432	-	0.1976
Radial Medium Blanket No. 2	-	7.849	1.511	-	-	0.4432	-	-
Axial Medium Blanket No. 1	-	7.525	1.468	-	-	0.4460	-	0.2134
Axial Medium Blanket No. 2	-	7.902	1.532	-	-	0.4413	-	-
Radial Coarse Blanket	-	11.309	0.5735	-	-	-	-	-

III. THE CRITICAL EXPERIMENT PROGRAM

The experimental program was planned by Atomic Power Development Associates, Inc., in conjunction with Argonne National Laboratory. At the latter's request, it was decided to perform the experiments on a simplified mockup of the Fermi reactor, since they would be of general interest to others working in the fast-reactor field. The fuel subassemblies were homogenized with the safety and control channels into a uniform composition, and the surrounding blanket was relatively uniform. This led to the compositions of Table II and configurations of Figs. 16 and 17 as the basic critical assembly.

The program had two main objectives:

1. to determine the amount of U^{235} required for criticality in this basic assembly, i.e., to determine the core size; and
2. to obtain experimentally the basic data needed for Core B temperature and power coefficients, i.e., to determine the local worths of fully enriched uranium and sodium in the core.

Further objectives were:

3. to determine the distributed worths of the other core materials to allow for materials discrepancies between the critical assembly and Fermi Core B;

4. to obtain the reactivity effects of various engineering features of Core B such as end gaps, safety and control channels, and rods;

5. to determine the heterogeneity effect of the fuel in this core and other reactivity effects, such as axial core expansion and oscillator rod;

6. to measure the spectral indices and the important reaction rates.

Finally, to provide for a significant underestimate of reactivity, it was planned:

7. to determine the amount of nickel reflector, replacing radial fine blanket, necessary for criticality on the 600-liter core (this reflector would then be in place for items 2 through 6 above);

8. to investigate the relative reactivity worths of various other reflectors.

IV. THE CRITICAL EXPERIMENT

Essentially two critical experiments were performed, the first with the compositions and regions as described above (Table II), except with a large core; the second with the core size reduced to the Fermi nominal size (600 liters) and the addition of a nickel reflector.

A. Critical Experiment without Nickel Reflector

1. Approach to Critical

After first loading the blankets and core outlines, as shown in Figs. 16 and 17, with fuel columns only in the inner radial half of the core volume and aluminum columns in place of fuel in the outer core volume, the approach to critical was made by replacing these aluminum columns in steps with columns of fully enriched uranium. The inverse count rate is plotted against U^{235} mass in Fig. 18, and the ratio of mass to count rate versus U^{235} mass is shown in Fig. 19. Criticality was achieved with a U^{235} loading of 507.4 kg in the 666.7-liter core shown in Fig. 20.

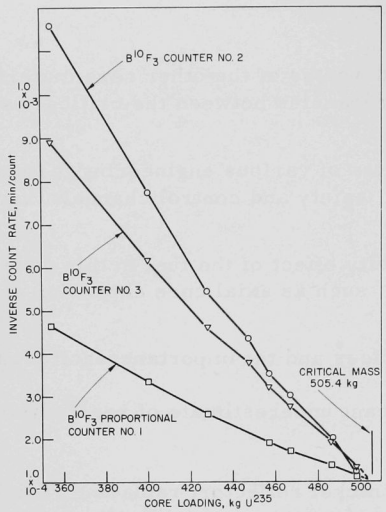

Fig. 18. Approach to Criticality without Nickel Reflector; Inverse Power Versus U^{235} Loading

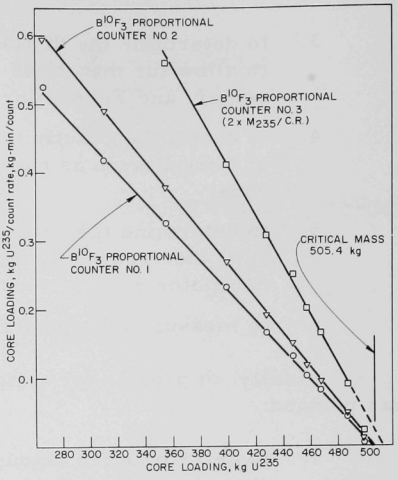

Fig. 19. Approach to Criticality without Nickel Reflector; Inverse Power x U^{235} Loading Versus U^{235} Loading

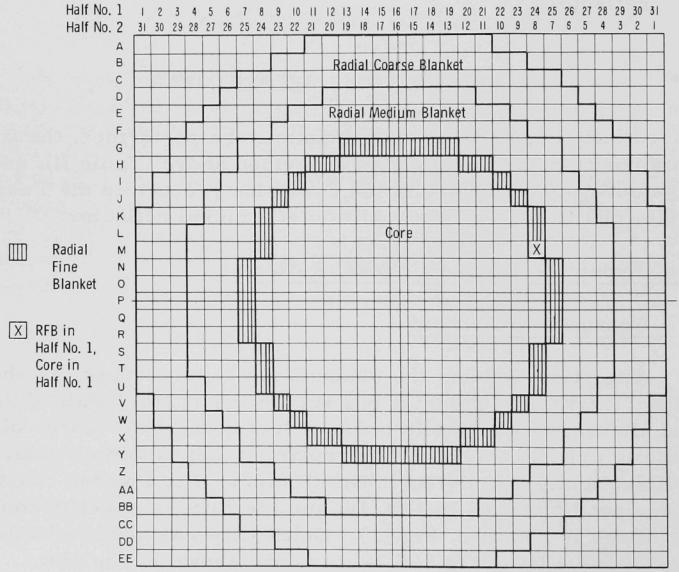

Fig. 20. Interface View of Assembly with 667-liter Core

The compositions of all the regions in this assembly are given in Table II. The basic ZPR-III and materials specifications used in the calculation are given in Appendix A. Table III gives the main dimensions of the assembly.

Table III

MAIN DIMENSIONS OF CRITICAL ASSEMBLY

The dimensions given for the core, radial fine blanket and axial fine blanket refer to their configurations with the 666.7-liter core. Their radii changed for the 599.3-liter core, as given in the text. All other regional dimensions are common to both core sizes. See Figs. 16 and 17.

Region	Core	Radial Fine Blanket	Axial Fine Blanket	Radial Medium Blanket No. 1	Radial Medium Blanket No. 2	Axial Medium Blanket No. 1	Axial Medium Blanket No. 2	Radial Coarse Blanket
Equivalent[1] Outer Radius (in.)	18.95	20.91	18.95	27.74	27.74	20.91	20.91	34.65
Axial Length[2] (in.)	18.03	21.03	3.00	21.03	10.50	7.30	4.00	28.00
Volume[3] (liters)	666.7	168.5	67.5	720.3	359.6	164.2	90.0	1237.9

(1)The equivalence is on an area basis.
(2)The lengths given are those in one assembly half.
(3)The volumes given are for the complete assembly.

2. Control-rod Calibration

Rod No. 10 (see Fig. 16) was generally used as the operating control rod in all experiments with this assembly. It was calibrated by the usual period measurements corresponding to an incremental change in rod position. The details of the inhour curve used for converting these periods to reactivity are given in Appendix B. The calibration curve thus derived is given in Fig. 21.

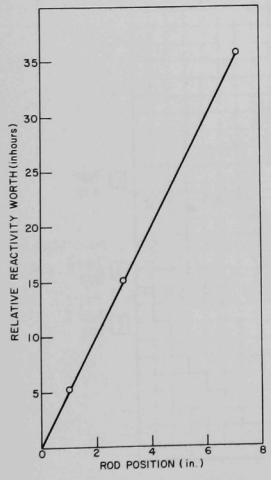

Fig. 21. Calibration of Control Rod No. 10 in 667-liter Core

3. Measurements of Edge Worth and Critical Mass

The 507.4-kg U^{235} loading of the assembly was 35.8 inhours supercritical with all rods fully inserted. A measurement of the worth of a core drawer containing 1.223 kg U^{235} relative to a radial fine blanket drawer at the core edge was made and found to be 18.3 Ih/kg U^{235}. From this we get the critical mass of the assembly at 25.1°C as 505.4 kg U^{235}. Through use of the core uranium density of Table II, a critical volume of 664.6 liters is obtained.

Since a core volume as large as this cannot be accommodated in the Fermi reactor, no further experiments were made on it. It was decided to reduce the core volume to 600 liters (the maximum size in the Fermi reactor) and reach criticality by the substitution of nickel reflector for radial fine blanket around the core.

B. Critical Experiment with Nickel Reflector

1. Approach to Critical

Sufficient core drawers were first replaced by radial fine blanket at the core edge to reduce the core volume to 599.3 liters. The core outline was made more uniform by the use of partial drawer loadings in some edge locations, as shown in Fig. 22. The compositions of this core and fine blankets were slightly different than the large core above and are given in Table IV. The composition of the radial fine blanket when criticality was achieved with the nickel reflector (Fig. 22) is that given in this table. The core contained 456.95 kg U^{235}. The approach to critical was made by stepwise substitution of Type "A" nickel-reflector drawers, as shown in Fig. 23, with composition 5.44 g/cc Ni, 0.159 g/cc Na, and 0.954 g/cc stainless steel, for radial fine blanket drawers around the core boundary. A plot of the inverse count rate versus number of reflector drawers is shown in Fig. 24. Its zig-zag shape is due mainly to the varying worth of a reflector drawer, depending on how much of its total area is in contact with the core.

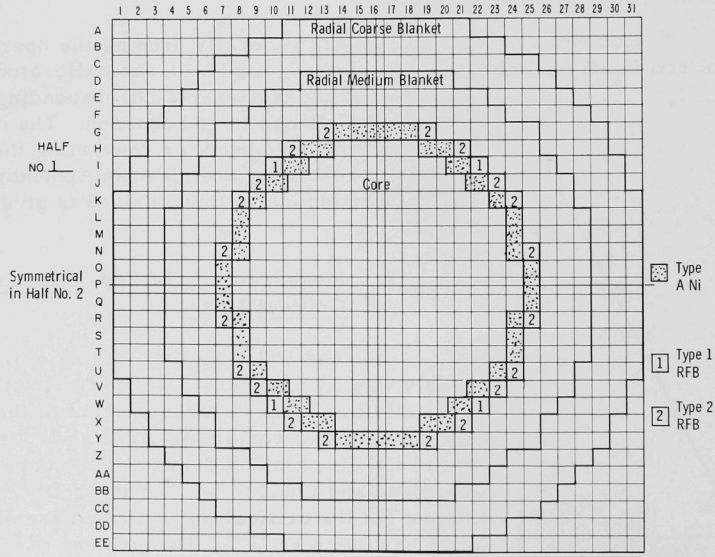

Fig. 22. Assembly with 599-liter Core and Critical Type "A" Nickel Radial Reflector - Low Worth Control Rods

Table IV

REGIONAL COMPOSITIONS (g/cc) OF CORE, FINE BLANKETS, AND NICKEL REFLECTOR IN NICKEL-REFLECTED ASSEMBLY (599-liter Core)

Region	93.2% Enriched Uranium	0.21% Depleted Uranium	Stainless Steel	Iron	Sodium	Oxygen	Molybdenum	Nickel
Core	0.8182**	-	3.625	0.2663	0.2987	0.1061	-	-
Radial Fine* Blanket	-	7.660	1.607	-	0.2523	-	0.2223	-
Axial Fine Blanket	-	7.559	1.500	-	0.3047	-	-	-
Radial Nickel* Reflector	-	-	0.9595	-	0.1608	-	-	5.421

*These are the average compositions of the configurations in Fig. 22. A single, Type "A," nickel-reflector drawer contains 5.443 g/cc Ni, 0.1594 g/cc Na, and 0.9544 g/cc stainless steel.

**This figure pertains to the core with unseeded control rods.

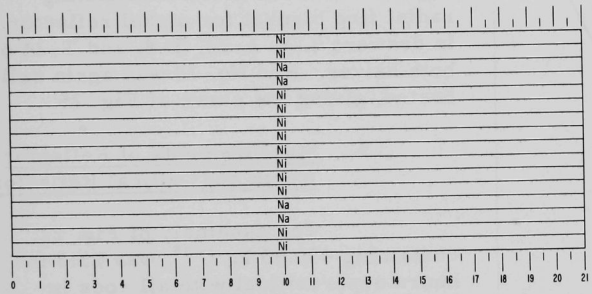

Fig. 23

Nickel-reflector Drawer, Type "A"

Fig. 24

Approach to Criticality with 599-liter Core by Addition of Type "A" Nickel Reflector

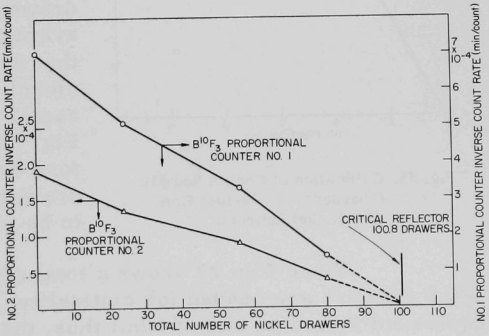

The nickel-reflector configuration at criticality is shown on Fig. 22. Its composition, given in Table IV, was slightly different from that given above because of edge drawers common to both core and reflector.

2. Control-rod Calibration

Control rod No. 10 was recalibrated in this core. The details of the inhour curve are given in Appendix B. The two control rods were then seeded by adding 1.311 kg of fully enriched uranium to each in place of 0.56 kg of steel, in order to increase the amount of subcriticality with both halves together and the control rods withdrawn, and to allow greater reactivity changes in the later experiments. The 599.3-liter core now contained 459.39 kg U^{235}. (Note that the core composition given in Table IV refers to the basic core with unseeded control rods; the seeding increases the enriched uranium density to 0.8225 g/cc and causes a negligible steel change.) The reflector shown on Fig. 22 was reduced by substituting radial fine blanket for nickel reflector in drawers L-8, L-24, T-8, and T-24 of both halves. Rod No. 10 was again calibrated, giving the curve of Fig. 25.

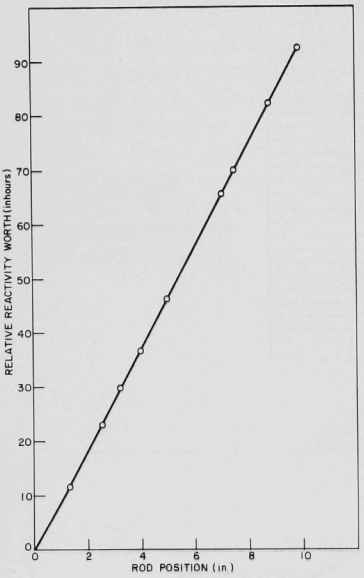

Fig. 25. Calibration of Control Rod #10 ("Seeded") in 599-liter Core with Nickel Reflector

3. Measurements of Reflector Worth and Critical Reflector

The assembly of Fig. 22, containing 456.95 kg U^{235}, was 23.3 inhours supercritical with all rods inserted. A series of experiments was performed with individual and groups of drawers in the nickel reflector to get an average worth per drawer. It was found that the average worth of a Type "A" nickel reflector drawer substitution for radial fine blanket in the reflector of Fig. 22 was 10.1 inhours. It would therefore be necessary to remove 2.3 reflector drawers of average worth from Fig. 22 to be just critical with all rods in.

Since Fig. 22 shows a total of 103.1 drawers for both halves, 100.8 drawers are needed for criticality. The 599.3-liter core has an equivalent diameter of 35.94 in.; thus, the critical Type "A" nickel reflector is equivalent to a 2.01-in.-thick annulus. The equivalence is on an area basis.

Using the average worth of 10.1 inhours per drawer, the worth of this critical reflector is readily found to be 1016 inhours. Later experiments on the worth of enriched uranium columns showed that 106 inhours were added to the assembly by seeding the two control rods. Hence, the critical Type "A" nickel reflector with seeded control rods fully inserted is worth 910 inhours and has an equivalent thickness of 1.78 in.

Reactivity compensation of later experiments was accomplished in general by adjustment of this nickel reflector. Rather than describe or sketch the reflector for each experiment, its equivalent annular thickness will be given. For some experiments a sketch is given, but it generally shows the critical nickel reflector with seeded control rods, the experimental thickness being given in the text. In all following experiments the control rods had the seeded composition.

V. ENGINEERING FEATURES OF FERMI CORE B

To establish the critical mass of the Fermi Core B reactor, one must consider the reactivity effects of the most important differences between it and the simplified mockup in ZPR-III. The differences due to the engineering features of end gaps, axial UO_2 blankets, and center gap are treated in this section. The remaining engineering features to consider, the safety and control channels, are treated in Section VII.

A. Reactivity Effect of End Gaps

The end gaps of the Fermi reactor, shown in Fig. 3, and with composition given in Table I, were simplified in the experiment to a representative one 3 in. long with an average composition of 0.5276 g/cc Na and 2.547 g/cc stainless steel. This composition was substituted in steps for half an axial fine blanket as shown in Fig. 26. The equivalent reflector thickness was 1.73 in.

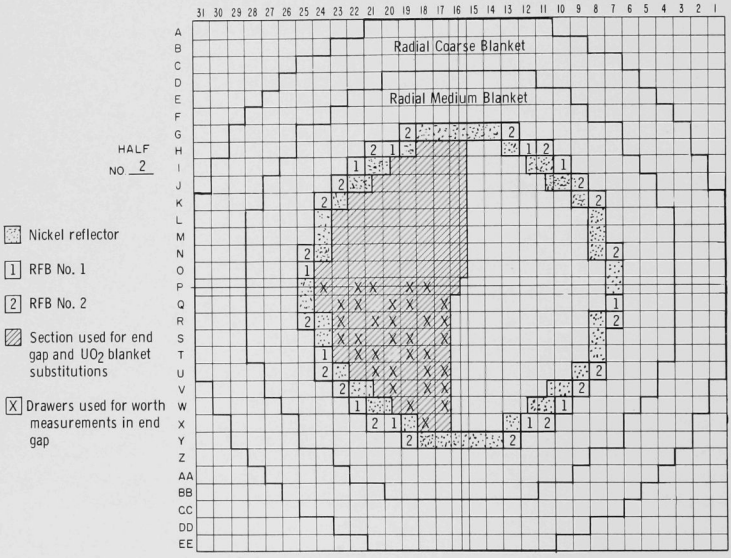

Fig. 26. Assembly Configuration for End Gap and UO_2 Axial Blanket Experiments

The average composition of the blanket removed was 7.361 g/cc depleted uranium, 0.2991 g/cc sodium, and 1.465 g/cc stainless steel. This substitution resulted in a reactivity increase of 8.9 inhours. Assuming that a full end gap would double this value, its worth is 17.8 inhours.

Further experiments were performed to obtain the distributed worths of various materials in this end gap to correct for materials discrepancies between the Fermi and experimental end gaps. Values obtained were +8.4 Ih/kg for sodium, +1.6 Ih/kg for stainless steel, +0.3 Ih/kg for depleted uranium, and +1.9 Ih/kg for nickel. The equivalent nickel-reflector thickness was 1.78 in.

B. Reactivity Effect of UO_2 Axial Blankets

As described in Section I, the Fermi reactor has upper and lower axial blankets that differ mainly in the provision of a meltdown region containing only sodium in each subassembly of the lower blanket. The two different geometries were mocked up to determine possible streaming effects.

The end gap mentioned in Section V, A was left in place for these experiments, and the UO_2 blankets mocked up behind it, i.e., in the region noted in Fig. 26. These UO_2 blankets replaced the axial medium blankets No. 1 and 2 which have a total length of 11.3 in. (see Table III). The drawer loading used for the upper UO_2 blanket is shown in Fig. 27; the materials are seen to be uniformly distributed. To mock up the lower UO_2 blanket with its central sodium region, a three-drawer unit module was necessary. Even then some difficulty was experienced, as the Fermi lower UO_2 blanket contains a 1.5-in.-square sodium region in a 2.69-in.-square subassembly. The square pitch of the ZPR-III matrix is 2.18 in. (see Appendix A), so the rectangular arrangement of the three-drawer unit module was necessary. These three drawers, two of which are identical, are shown in Figs. 28 and 29. Together they have an area of 14.25 in.^{2} and represent the area of two Fermi subassemblies (14.48 in.^{2}). Their two sodium regions, each 2.25 in.^{2} in area (in the two identical drawers), represented the two sodium regions of the two Fermi subassemblies, each of which is also 2.25 in.^{2} in area. This three-drawer unit module was loaded in a repetitive pattern into the region shown in Fig. 26.

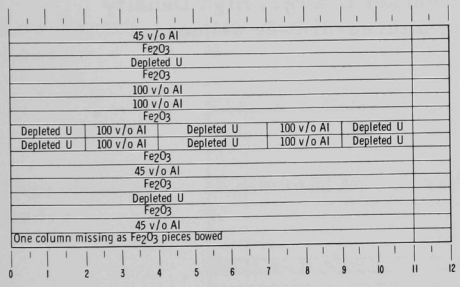

Fig. 27. Upper UO_2 Axial Blanket Drawer, High Density

These two axial blankets, the upper UO_2 one of Fig. 27 and the lower UO_2 one of Figs. 28 and 29, were substituted in turn for axial medium blankets No. 1 and 2 in the experimental region. The compositions of

the latter are available from Table II. The compositions of the UO_2 blankets, as well as the experimental results, are given in Table V. The area of the complete blanket was twice that of the experimental region of Fig. 26; this factor is used in extrapolating the measured reactivity changes in the substitutions to the complete blanket. The equivalent nickel-reflector thickness was 1.73 in.

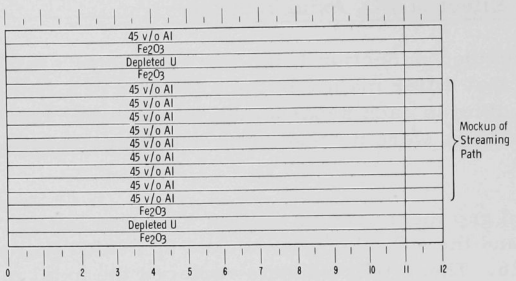

Fig. 28. Lower UO_2 Axial Blanket Drawer, High Density (Represents two of a three-drawer sequence)

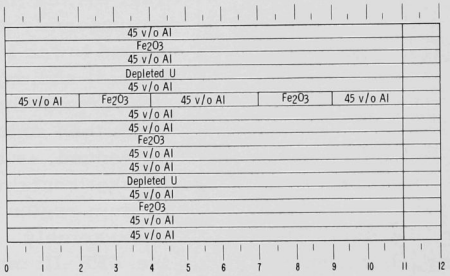

Fig. 29. Lower UO_2 Axial Blanket Drawer, High Density. (Represents one of a three-drawer sequence)

These experiments were then repeated with the depleted uranium and oxygen density reduced by half approximately, the aluminum and stainless steel being correspondingly increased and the iron reduced. The equivalent nickel-reflector thickness varied between 1.73 and 1.82 in. The results of the experiments with these low-density blankets are given in Table V along with those of the initial high-density blankets. These experiments separate the streaming effect to some extent, as the densities

in the low-density, upper UO_2 blanket are approximately the same as those in the high-density, lower UO_2 blanket. An approximate correction is applied for the materials discrepancies below.

Table V

RESULTS OF UO_2 AXIAL BLANKET EXPERIMENTS

Axial Blanket			Worth Complete Blanket Relative to AMB No. 1 & 2, Ih
Type	Composition, g/cc		
Low-density Upper	Depleted U	1.526	-44.4
	O	0.2036	
	Al	0.6220	
	Stainless Steel	1.058	
	Fe	0.5108	
Low-density Lower	Depleted U	0.9315	-98.4
	O	0.1319	
	Al	0.7203	
	Stainless Steel	1.484	
	Fe	0.3309	
High-density Lower	Depleted U	1.863	-54.1
	O	0.2576	
	Al	0.6020	
	Stainless Steel	0.7397	
	Fe	0.6463	
High-density Lower with Ni in Front 3.3 in.	Front 3.3 in.		
	Ni	1.650	-15.9
	Al	0.5692	
	Stainless Steel	1.427	
	Back 8 in.		
	Depleted U	1.913	
	O	0.2626	
	Al	0.6204	
	Stainless Steel	0.7066	
	Fe	0.6588	
High-density Upper	Depleted U	3.038	+47.9
	O	0.4152	
	Al	0.5392	
	Stainless Steel	0.7396	
	Fe	1.042	

Table V (Cont.)

Axial Blanket			Worth Complete Blanket Relative to AMB No. 1 & 2, Ih
Type	Composition, g/cc		
	Front 2.3 in.		
High-density Upper with Ni in Front 2.3 in.	Ni	2.370	+90.6
	Al	0.4475	
	Stainless Steel	1.676	
	Back 9 in.		
	Depleted U	3.181	
	O	0.4256	
	Al	0.5627	
	Stainless Steel	0.7065	
	Fe	1.068	
	Front 4.3 in.		
High-density Upper with Ni in Front 4.3 in.	Ni	2.535	+117.4
	Al	0.5498	
	Stainless Steel	1.654	
	Back 7 in.		
	Depleted U	3.274	
	O	0.4242	
	Al	0.5328	
	Stainless Steel	0.7066	
	Fe	1.064	

Finally, experiments were performed on the worth of a nickel reflector replacing the first few inches of both the high-density upper and high-density lower UO_2 blankets, to cover its possible use in the Fermi reactor. Nickel-reflector compositions, given in Table V, were used in the front 3.3 in. of the high-density lower UO_2 blanket, and in the front 2.3 in. and 4.3 in. of the high-density upper UO_2 blanket. The various results are given in Table V. The equivalent radial nickel-reflector thickness was 1.73 in. with the lower blanket and 1.62 in. with the upper blanket. It should be noted that Table V refers all reactivity changes to the axial medium blankets No. 1 and 2, extrapolated to the full blanket area.

The following results can also be derived from the experiments in Table V.

1. Worth of Axial Nickel Reflectors

Replacing the front 3.3 in. of the high-density lower UO_2 blanket with the given nickel-reflector composition results in a reactivity increase of 54.1 - 15.9 = 38.2 inhours. Similar results for the front 2.3 in. and 4.3 in. of the high-density upper UO_2 blanket are 90.6 - 47.9 = 42.7 inhours and 117.4 - 47.9 = 69.5 inhours, respectively.

2. Reactivity Effect of Streaming Paths

The high-density lower UO_2 blanket is worth approximately 10 inhours less than the low-density upper UO_2 blanket. No experimental values are available for distributed reactivity worths in this region, but a correction for materials discrepancies can be applied from adjusted calculated values. This correction shows the high-density lower blanket is 9 inhours more reactive than the low-density upper due to composition differences. Consequently, a negative reactivity effect of approximately 19 inhours can be ascribed to the streaming paths in the complete lower blanket.

C. Reactivity Effect of Central Gap

The Core B design for the Fermi reactor is such that no fuel is present in a $\frac{1}{2}$-in. central gap extending across the core. It is shown in Fig. 3 as Region F. Its purpose is to provide structural support for the fuel-element bundles, and it contains only sodium and stainless steel (to the extent of 0.0949 g/cc sodium and 7.082 g/cc stainless steel).

This gap was mocked up in the front $\frac{1}{2}$ in. of the drawers shown in Fig. 30. The equivalent nickel-reflector thickness varied between 1.82 and 1.90 in. The gap was not symmetrically placed relative to the midplane but $\frac{1}{2}$ in. to one side of it. This simplification leads to no great error. The existing sodium and stainless steel of these drawers (see Figs. 6-13) were left in place, and the enriched uranium and iron oxide columns displaced axially by inserting $\frac{1}{2}$-in.-long stainless steel shims at the front. If the drawer front plate is included in this region (giving a 0.53-in. gap measured from the midplane) it has the following composition:

Before recessing of fuel and iron oxide columns;

93.2% Enriched Uranium	0.8142 g/cc
Oxygen	0.1027
Sodium	0.2936
Stainless Steel	3.914

After recessing of fuel and iron oxide columns;

Sodium	0.2936 g/cc
Stainless Steel	4.588

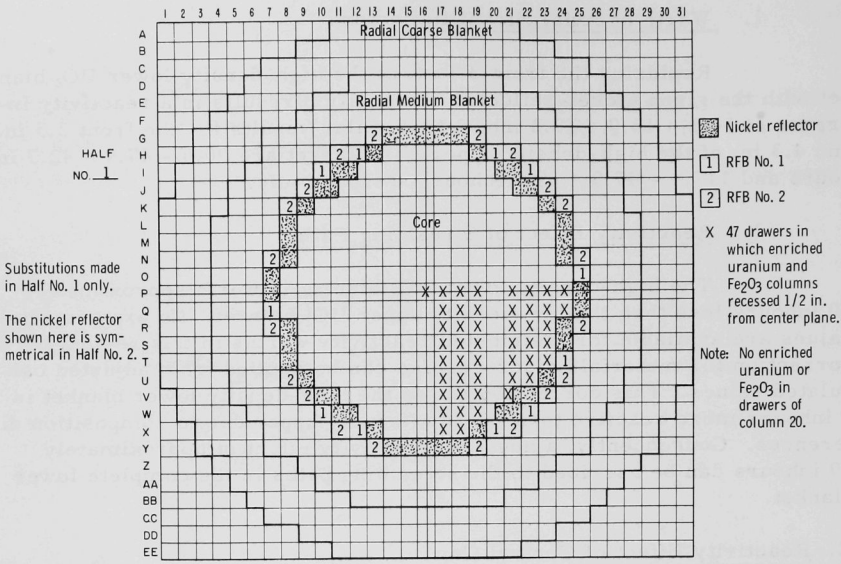

Fig. 30. Assembly Configuration for Center Gap Experiment

This substitution resulted in a reactivity decrease of 59.8 inhours. Since one-quarter of the fuel columns were recessed, a linear extrapolation of this result to the full core gave a reactivity loss of 239.2 inhours. There are two principal sources of error in the experiment:

1. The sodium and stainless steel columns of the core were not recessed $\frac{1}{2}$ in. This meant, in effect, that depleted uranium instead of stainless steel was present in the $\frac{1}{2}$ in. of the extended core at its axial edge.

2. The composition of the central gap mockup was appreciably different from that of the Fermi reactor.

Both of these errors caused the measured reactivity loss to be too high. From a knowledge of the measured reactivity worths of various materials (see Section IX) the first error is approximately 17 inhours and the second approximately 25 inhours (both for the full core).

Hence, the reactivity loss caused by the $\frac{1}{2}$-in. central gap in the Fermi reactor is approximately 239 - 42 = 197 inhours.

D. Antimony-Beryllium Source

In the Fermi reactor the antimony-beryllium neutron source occupies a subassembly at the core radial edge (see Fig. 2). The beryllium is in the shape of an annular cylinder, 25 in. long, 1 in. in ID, and 2.5 in. in OD. A mockup was made in Assembly 35 of this beryllium component, and its effects were determined. Drawer P-8 and the adjacent half of P-9 in both machine halves were chosen to represent the subassembly and these were first loaded to contain average core composition (as in the safety channel experiment). In the beryllium mockup a 26-in. length was used, and the beryllium was arranged as illustrated in Fig. 31 to approximate an annular shape. The equivalent nickel-reflector thickness was 1.90 in. This mockup was substituted for the average core material in the "channel" with a resulting reactivity gain of 8.6 inhours. Table VI gives the essential details of the substitution.

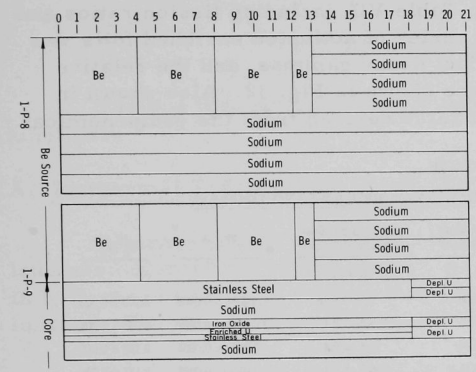

Fig. 31. Half #1 Drawer Loadings of Beryllium-source Mockup

Table VI

BERYLLIUM-SOURCE EXPERIMENT: COMPOSITION CHANGES IN "SOURCE CHANNEL"
(Cross Section: 7.26 in.^{2})

	Axial Regions	Composition
Before Substitution	Core, -18 to + 18 in.	0.824 g/cc Enriched Uranium, 0.111 g/cc Oxygen, 0.295 g/cc Sodium, 0.280 g/cc Iron, 0.356 g/cc Stainless Steel
	Fine Blanket, -18 to -21 in. and +18 to +21 in.	7.67 g/cc Depleted Uranium, 0.230 g/cc Molybdenum, 0.265 g/cc Sodium, 1.468 g/cc Stainless Steel
After Substitution	Source Beryllium Component -13 to +13 in.	0.509 g/cc Beryllium, 0.213 g/cc Sodium, 0.801 g/cc Stainless Steel
	Sodium Channel -13 to -21 in., +13 to +21 in.	0.628 g/cc Sodium, 1.68 g/cc Stainless Steel

With the source mockup in place, foils of enriched and natural uranium were irradiated at several radial positions near the reactor midplane to obtain fission and capture rates near the beryllium as compared with rates at the core center. The equivalent nickel-reflector thickness was 1.84 in. One series of enriched-natural foil sets was analyzed radiochemically; the results are given in Table VII, including fission ratios and capture-to-fission ratios. Another series of activated enriched foils was analyzed by counting of fission product decay gammas, and the relative activations as a function of radius are shown in Fig. 32. Also shown in Fig. 32 are the relative U^{235} fission rates derived from the radiochemical data.

Table VII

RADIOCHEMICAL ANALYSIS OF FOILS IRRADIATED FOR BERYLLIUM-SOURCE EXPERIMENT

Foil Set #	Radius (in.)[1]	Fissions per Gram Enriched Uranium[2] (x 10^9)	Fissions per Gram Depleted Uranium[3] (x 10^8)	Captures per Gram Depleted Uranium[3] (x 10^8)	$\sigma_f^{28}/\sigma_f^{25}$	$\sigma_c^{28}/\sigma_c^{25}$
1	22.85	7.17 ± 0.21	0.60 ± 0.06	5.31 ± 0.16	0.0034 ± 0.0008	0.070 ± 0.003
2	21.84	8.50 ± 0.25	0.93 ± 0.05	5.67 ± 0.17	0.0059 ± 0.0007	0.063 ± 0.003
3	20.83	11.8 ± 0.3	1.32 ± 0.04	13.4 ± 0.4	0.0061 ± 0.0004	0.108 ± 0.005
4	15.28	25.2 ± 0.8	5.14 ± 0.15	36.5 ± 1.1	0.0149 ± 0.0009	0.137 ± 0.006
5	14.30	22.3 ± 0.7	5.94 ± 0.18	23.1 ± 0.7	0.0209 ± 0.0011	0.098 ± 0.005
6	13.12	19.4 ± 0.6	6.32 ± 0.19	22.0 ± 0.7	0.0267 ± 0.0014	0.108 ± 0.005
7	0.25	25.1 ± 0.8	9.88 ± 0.29	21.8 ± 0.7	0.0333 ± 0.0018	0.082 ± 0.004
8	-0.25	23.8 ± 0.7	10.3 ± 0.3	22.6 ± 0.7	0.0371 ± 0.0020	0.090 ± 0.004
9	-20.83	8.85 ± 0.27	1.24 ± 0.04	8.88 ± 0.26	0.0088 ± 0.0006	0.095 ± 0.004
10	-21.84	7.31 ± 0.21	0.80 ± 0.04	5.49 ± 0.16	0.0058 ± 0.0007	0.071 ± 0.003
11	-22.85	6.03 ± 0.18	0.59 ± 0.04	4.46 ± 0.15	0.0047 ± 0.0008	0.070 ± 0.003

[1]Beryllium source between radii + 15.3 in. and + 18.6 in.

[2]Enriched uranium = 93.21 w/o U^{235}

[3]Depleted uranium = 0.485 w/o U^{235}

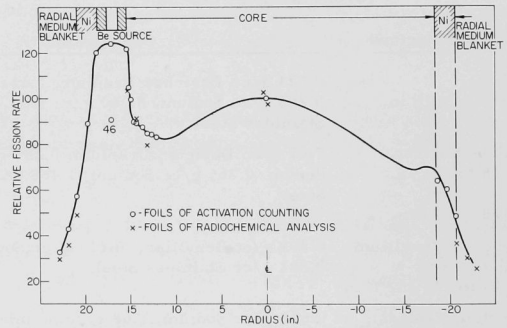

Fig. 32. Fission Rates of Enriched Uranium at Midplane in Beryllium-Source Experiment

The graph shows an increase of up to 25% in the U^{235} fission rate near the beryllium source relative to the fission rate at the core center. Also, Table VII shows a U^{238} capture rate near the beryllium which is 165% that of the core center.

VI. KINETICS FEATURES

Various measurements were made in connection with reactor kinetics.

A. Isothermal Temperature Coefficient

A measurement of the reactivity of the assembly with two identical loadings but different temperatures was made. The nickel reflector present in both cases had an equivalent thickness of 1.73 in. with the normal core loading. The temperature difference was 6°C.

The measurements result in an isothermal temperature coefficient of reactivity of -1.1 Ih/°C.

B. Reactivity Effect of Axial Core Expansion

The greatest contribution to the reactivity effect of core expansion comes from the axial expansion of the fuel. Hence, an experimental check on the value can be obtained by expanding only the fuel columns.

Since the expansion takes place into the end-gap region of the Fermi reactor, the mockup of this region (see Section V) was in place for the experiment. All enriched uranium and neighboring iron oxide columns within the end-gap outline of Fig. 26 were expanded, by 0.1504 in., by inserting 0.0376-in.-thick stainless steel shims in the columns at axial distances of 3, 7, 11, and 15 in. from the central plane. In Fermi Core B this expansion would be equivalent to a uniform temperature rise of 515.8°C, assuming a temperature coefficient of linear expansion of 16.2×10^{-6}/°C for the UO_2-stainless steel cermet.

Extrapolation of the results to the full core size and correction for the reactivity effect of the stainless steel shims led to a temperature coefficient of reactivity due to axial expansion of $-4.9 \times 10^{-6} \Delta k/k/°C$ for a uniform temperature increase over the whole core.

C. Measurement of Rossi-Alpha

Using the technique described by Brunson et al.,[4] the Rossi-alpha value, $\alpha = -\beta_{eff}/\ell$, at delayed critical was obtained. The assembly configuration is shown on Fig. 33; the reflector was composed mainly of the usual nickel and partly of a nickel oxide composition.

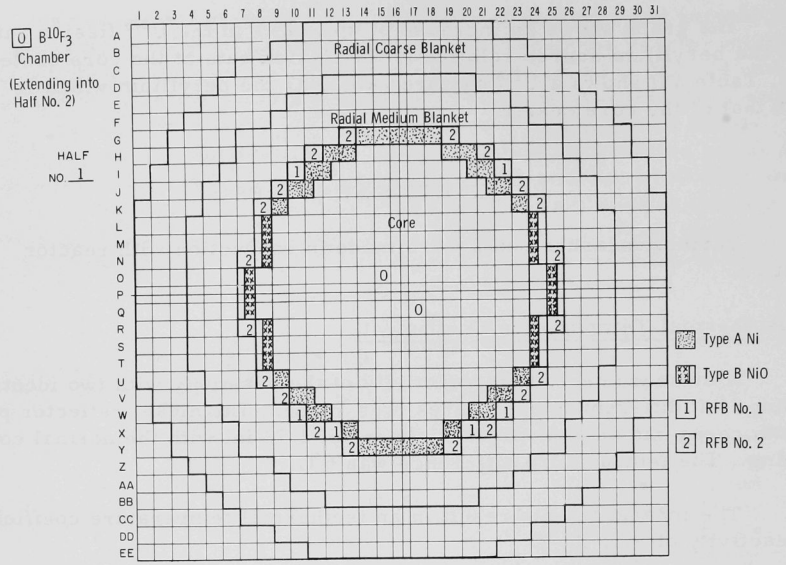

Fig. 33. Assembly Configuration for Rossi-Alpha Measurements

Values of alpha were measured at three subcritical points. Extrapolation to delayed critical gave a value of $\alpha = -1.59\ (\pm 0.03) \times 10^{4}\ \text{sec}^{-1}$. When a value of β_{eff} of 6.65×10^{-3} (see Appendix B) was used, the prompt neutron lifetime ℓ was found to be 4.18×10^{-7} sec. This compares well with the calculated value of 3.97×10^{-7} sec in Appendix B.

VII. SAFETY AND CONTROL CHANNELS AND RODS; OSCILLATOR ROD

The basic critical assembly contains no safety or control-rod channels. The compositions were homogenized along with that of the fuel region to give the uniform composition of the mockup. The reactivity effect of these channels is quite high and justifies an experimental determination.

A. Reactivity Worths of Safety and Control Channels

Figure 3 shows a safety-rod channel at an average radius of 7.16 in. with an area of 7.24 in.^{2}. It was mocked up in the assembly as a rectangular channel in drawers P-19 and adjacent half of P-20 (see Fig. 34), giving an average radius of 7.10 in. and an area of 7.16 in.^{2},

extending through the entire core and both axial blankets. The normal experimental axial blankets with compositions of Table II were in place for these experiments. In the safety-channel region, however, the core and blanket compositions were first rearranged to give values as close as possible to the average, rather than to that of the normal drawers in that position. The safety-channel mockup, consisting entirely of sodium cans, was substituted in steps for these average compositions. Table VIII shows the compositions involved in the substitution.

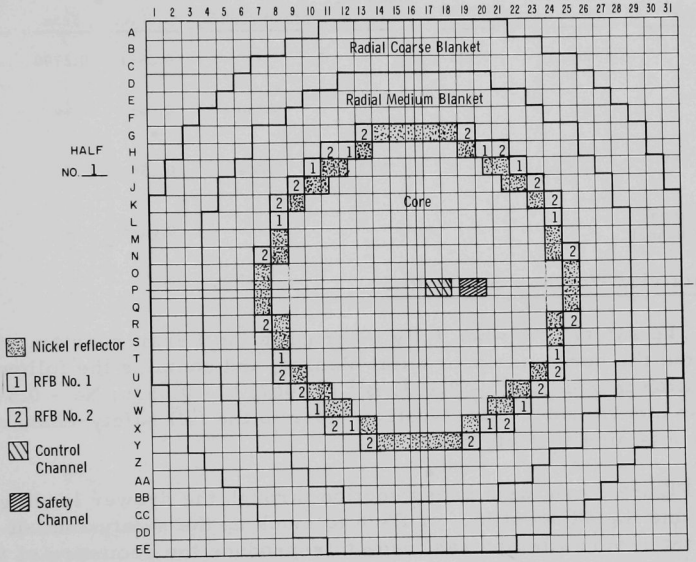

Fig. 34. Assembly Configuration for Reactivity Worths of Control and Safety Rods and Channels

A total reactivity loss of 186 inhours was measured for the substitution throughout the core and both axial blankets. Because of this large change, the radial nickel reflector was not constant for all steps of the experiment but varied between 1.76 and 2.05 in. The reflector shown in Fig. 34 is the critical one with seeded control rods.

The safety channel drawers P-19 and P-20 were then restored to normal configuration and the same experiment repeated for the control channel in drawers P-17 and adjacent half of P-18 (see Fig. 34). This gave an average radius of 2.63 in. and area of 7.16 in.^{2}, as compared with 2.69 in. and 7.24 in.^{2} in the Fermi reactor. Again, the regions extended through the entire core and axial blankets. The equivalent nickel-reflector

thickness varied between 1.99 and 2.12 in. The compositions involved in the substitution were the same as in the safety-channel experiment (see Table VIII), but this time the resulting total reactivity loss was 216 inhours.

Table VIII

COMPOSITIONS (g/cc) FOR THE SAFETY AND CONTROL-CHANNEL EXPERIMENTS; AVERAGE COMPOSITION IN BOTH SAFETY AND CONTROL CHANNEL REGIONS

Region	93.2% Enriched Uranium	Oxygen	0.21% Depleted Uranium	Molybdenum	Sodium	Iron	Stainless Steel
Core	0.8240	0.111	-	-	0.2951	0.2796	3.561
Axial Fine Blanket	-	-	7.67	0.230	0.265	-	1.468
Axial Medium Blanket	-	-	7.43	0.214	0.256	-	1.486
Safety Channel Control Channel	-	-	-	-	0.6276	-	1.676

B. Reactivity Worth of Safety Rod

The safety rod, when fully inserted in the Fermi reactor, extends throughout the core and upper axial blanket, and contains the following composition in g/cc: B^{10} - 0.123; B^{11} - 0.067; C - 0.0536; Na - 0.542; and stainless steel - 1.26. These values refer to the full safety-channel region containing a safety rod.

Figure 35 shows a cross section through the drawer loadings used in P-19 and the adjacent half of P-20 to mock up the safety rod. It will be noticed that some attempt was made to reproduce the geometry of the actual safety rod, which consists essentially of a hollow cylinder of enriched boron carbide clad in stainless steel and cooled by sodium. The composition in g/cc achieved in this mockup was B^{10} - 0.123; B^{11} - 0.084; C - 0.074; Na - 0.478; and stainless steel - 1.963, again referred to the full-channel region containing a safety rod.

The safety channel was first established by inserting sodium cans in P-19 and the adjacent half of P-20 throughout the core and axial blankets. Because of the high worth of the safety rod (approximately 600 inhours), it would be cumbersome to measure it in the normal manner in steps of, say, 50 inhours, and compensating for the reactivity loss by means of fuel and/or reflector addition. Furthermore, it would not represent conditions

in the actual reactor, where the safety rod is inserted without any compensating reactivity addition. A compromise was made by measuring the reactivity effect in one assembly half by the normal critical method, and in the other half by taking subcritical counts. This second method of determining reactivity worth is explained in Appendix C. Its basis is that at low amounts of subcriticality, multiplication of source neutrons is inversely proportional to this amount; the proportionality is essentially determined from a calibration made by removing a known amount of reactivity from the critical reactor, e.g., by withdrawing the calibrated control rod.

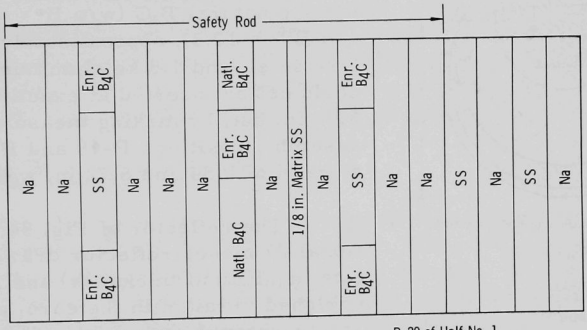

(In Half No. 2 the same columns are present, in reverse order.)

All columns shown are 1/4 in. thick.

This figure shows the materials used to mock up the safety rod. The materials in the right-hand side of drawer P-20 refer to the core drawers; in the axial blanket drawers the two 1/4-in.-thick columns of stainless steel were replaced by depleted uranium.

Fig. 35. Cross Section through Safety-rod Mockup

The composition of the safety rod was then substituted in place of the channel composition in a number of steps. The reflector shown in Fig. 34 was in place at the start of the substitution, but was increased by adding 27 nickel drawers during the initial steps, for which the reactivity worth of approximately half the safety rod was determined from the critical position. The equivalent nickel-reflector thickness varied between 1.91 and 2.40 in. Additional reactivity was gained by inserting 2.622 kg of fully enriched uranium in the core.

The results of the safety-rod-channel substitution gave 303.9-inhour loss for the core section of one assembly half by critical position, 307.2-inhour loss for the core section of the other assembly half by subcritical counts, and 14.5-inhour loss for the top axial blanket section by critical position. Hence, the total loss upon substitution of the safety-rod for the safety-channel composition was 625.6 inhour.

C. Reactivity Worth and Variation of Oscillator Rod

Stability tests on the Fermi reactor will be made by rotating an oscillator rod containing eccentrically loaded boron carbide in an outer safety rod channel with a radius of 8.07 in.

Figure 36 shows the mockup of the oscillator rod used in the experiment. Aluminum was used to mock up sodium, and the rectangular pieces of natural boron carbide were arranged to approximate the annular configuration of the Fermi oscillator rod. The radius of rotation of the boron carbide in the mockup was 0.44 in., as compared with 0.5 in. in the Fermi rod. The active section of the mockup was 35 in. long and contained 615.7 g natural B_4C (w/o B = 76.98; a/o B^{10} = 19.2), approximately 7.4 kg stainless steel, and 1.0 kg aluminum. This rod could not be inserted at exactly a radius of 8.07 in. but, by making measurements in assembly positions P-19 and P-20, values at radii of 6.54 and 8.72 in. were obtained.

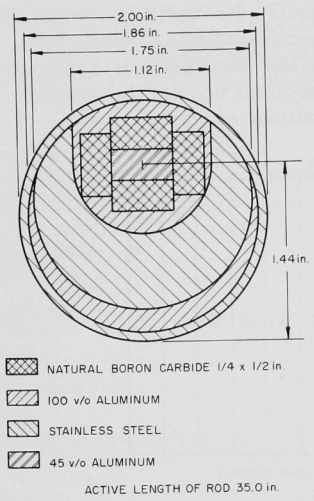

Fig. 36. Cross Section through Oscillator-rod Mockup

The reflector of Fig. 34, with an additional 27 nickel-reflector drawers (or 2.2 in. total equivalent thickness) and 2.622 kg fully enriched uranium in the core, and with the safety-channel composition in locations P-19 and adjacent half of P-20, was the configuration used for a reference critical measurement. The oscillator rod was then substituted for the sodium cans in P-19, and its worth determined from subcritical counts. Criticality was then achieved by adding an additional 5.244 kg fully enriched uranium to the core. A remotely controlled selsyn system allowed rotation of the rod to various angular settings, and the reactivity changes were found from the changing critical positions. Table IX gives the results; the reactivity variation of rod rotation is given in Fig. 37.

Table IX

REACTIVITY WORTH AND VARIATION OF THE OSCILLATOR-ROD MOCKUP

Experiment	Reactivity Worth, Ih
Substitution of Oscillator Rod for Safety Channel in P-19	-132.8
Rotation of Oscillator Rod in P-19	7.7 Peak-to-peak
Rotation of Oscillator Rod in P-20	8.8 Peak-to-peak
Substitution of Safety Channel for Oscillator Rod in P-20	+111.8

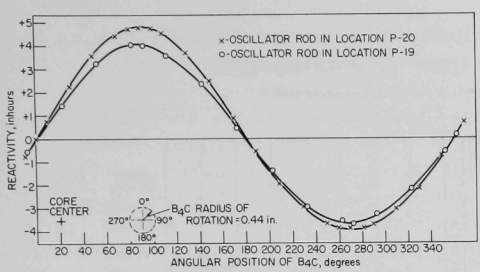

Fig. 37. Reactivity Response of Oscillator-rod Rotation

Location P-19 was then loaded with normal core and blanket materials, and P-20 completely filled with sodium cans. The 5.244 kg uranium added above were removed, and the above experiments with the oscillator rod were repeated in location P-20; i.e., the worth of the rod relative to safety-channel composition (from subcritical counts) and the reactivity variation of rod rotation (from critical position) were determined. The equivalent nickel-reflector thickness varied between 2.01 and 1.8 in. The results are again given in Table IX and Fig. 37.

D. Reactivity Worth of Control Rod

The control rod in the Fermi reactor is 10 in. long and contains 0.2648 g/cc boron carbide, 0.573 g/cc sodium, and 1.58 g/cc stainless steel, based on a 10-in.-long control-channel volume. The boron carbide is a hollow cylinder clad in stainless steel and cooled by sodium. Requirements were to find the cylinder worth as a function of boron enrichment when it was symmetrically placed in the core about the center plane, and also to find the worth of the fully enriched rod in the axial blanket, just touching the core.

Three boron enrichments were chosen for the experiment: fully enriched (high-worth rod); approximately 66% enriched (medium-worth rod); and approximately 43% enriched (low-worth rod), as shown in Fig. 38. It will be noticed that an attempt was made to mock up the rod geometry. The boron carbide content was 0.3479 g/cc for the high-worth rod, 0.3559 g/cc for the medium-worth rod, and 0.3640 g/cc for the low-worth rod, with 0.443 g/cc sodium, and 1.769 g/cc stainless steel in all three. Complete compositions are given in Table X.

A reference loading was made with control-channel composition (see Table VIII) in P-17 and the adjacent half of P-18 throughout the core and axial blankets. These three different rods were then substituted for the control channel in the central 10 in. of the core length, and the reactivity change was measured by a combination of critical position and subcritical counts. The nickel reflector shown in Fig. 34 was increased by a total of 12 drawers and the core fuel by 10.488 kg fully enriched uranium for these experiments. The equivalent nickel-reflector thickness was then 2.26 in. With the control-channel composition replaced in the core section, the high-worth rod was then substituted for the control channel in the 10-in.-length of axial blanket just behind the core. Table X gives the results of these experiments.

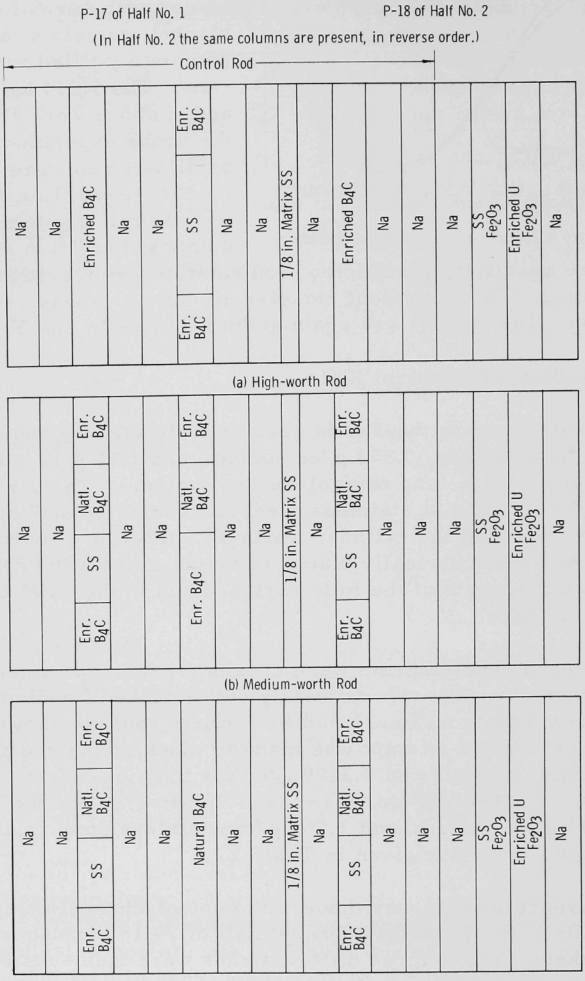

All columns shown are 1/4 in. thick. These figures show the materials used to mock up the three control rods in the core. The high-worth rod (a) was also inserted in the axial blanket; in the drawer section to the right of the "rod," depleted uranium columns were then in place of the Fe_2O_3 and enriched uranium columns.

Fig. 38. Cross Section through Control-rod Mockups

Table X

COMPOSITIONS AND REACTIVITY WORTHS OF VARIOUS CONTROL-ROD MOCKUPS

Control Rod Mockup									
		Composition, g/cc						Worth of Mockup Relative to Control Channel, Ih	Worth Measured by
Position	Type	B^{10}	B^{11}	C	Na	Stainless Steel	Impurity		
10 in. in Axial Blanket	High-worth	0.217	0.024	0.096	0.443	1.769	0.010	-29.7	Critical Position
10 in. in Core	High-worth	0.217	0.024	0.096	0.443	1.769	0.010	-476	Critical Position and Subcritical Counts
10 in. in Core	Medium-worth	0.167	0.088	0.093	0.443	1.767	0.008	-404	Subcritical Counts
10 in. in Core	Low-worth	0.118	0.152	0.089	0.443	1.767	0.005	-303	Critical Position

VIII. HETEROGENEITY EFFECT OF FUEL

The enriched uranium columns used in the core were $\frac{1}{8}$ in. thick, and an experimental determination of their heterogeneity effect on reactivity was necessary. It was also decided to check whether the nonuniform distribution of the iron oxide columns in contact with enriched uranium (see Figs. 6-13) had any effect on reactivity.

The normal axial blankets of Table II were in place for these experiments. First, the iron oxide columns in a wedge-shaped section of one assembly half, approximately the same as the section for the fuel-bunching experiments (see Fig. 39), were redistributed uniformly throughout the section. The equivalent nickel-reflector width was 1.71 in. A reactivity loss of 1.6 inhours was measured, or 19 inhours if extrapolated linearly to the full core size on a weight basis of iron oxide.

Without changing this redistributed iron oxide or the nickel reflector, the 36 $\frac{1}{8}$-in. columns (52.44 kg) of enriched uranium were bunched into eighteen $\frac{1}{4}$-in. columns in the wedge-shaped section of Fig. 39. Typical drawer-loading changes are shown in Fig. 40. No appreciable net radial movement of fuel occurred. A reactivity increase of 63.4 inhours was measured which, when linearly extrapolated to the core fuel loading with unseeded control rods (490.3 kg), gave 592.4 inhours on a weight basis of the enriched uranium.

To find the effect of unbunching the fuel into $\frac{1}{16}$-in.-thick columns, the normal $\frac{1}{8}$-in.-thick plates were restored to the bunched region except in the inner unbunching region of Fig. 39, in which 2 x $\frac{1}{16}$-in. columns were used. With this loading as a reference and with a nickel-reflector of 1.82-in. equivalent thickness, the fuel in this inner region (26.27 kg) was then unbunched into separate $\frac{1}{16}$-in.-thick columns as shown on Fig. 41.

A reactivity loss of 17.3 inhours was found, which extrapolated linearly to 323.6 inhours for the full core on a weight basis of enriched uranium.

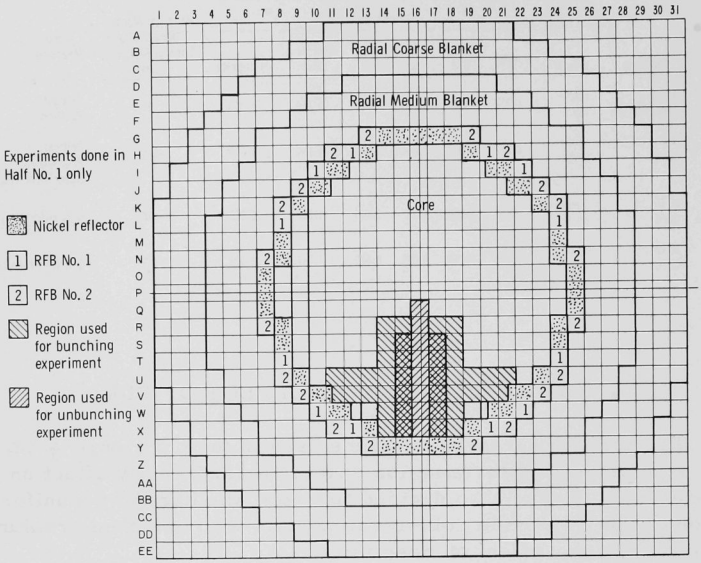

Fig. 39. Assembly Configuration for Fuel Heterogeneity Experiments

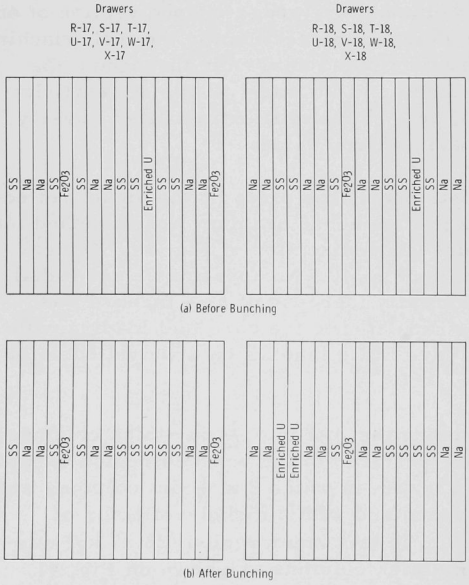

Fig. 40

Drawer Arrangements for Fuel-bunching Experiment

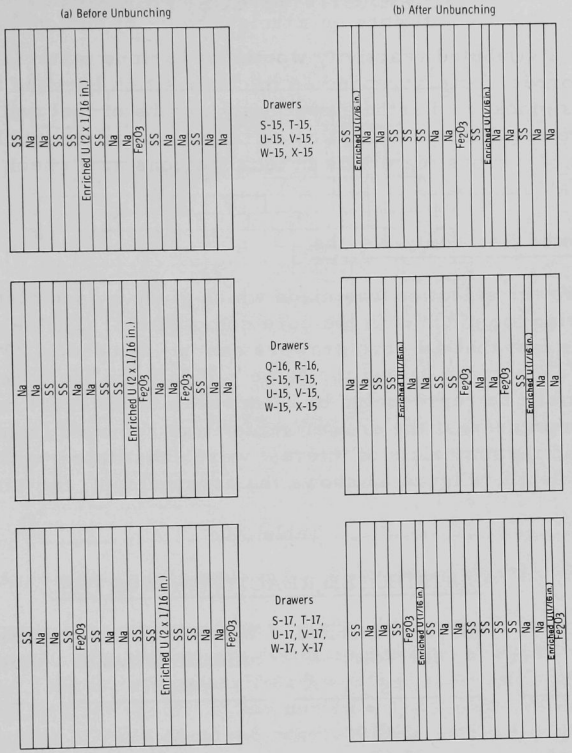

Fig. 41. Drawer Arrangement for Fuel-unbunching Experiment

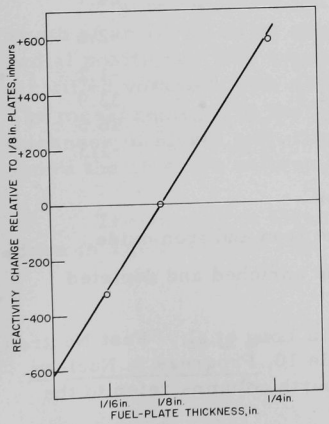

The results of these bunching and unbunching experiments are plotted in Fig. 42, for which the $\frac{1}{8}$-in.-thick fuel served as reference. Extrapolation of the curve to zero-fuel plate thickness led to the result that homogenizing the fuel in the full core would result in a reactivity loss of 612 inhours compared with the basic core arrangement with $\frac{1}{8}$-in.-thick plates and unseeded control rods.

Fig. 42. Results of Fuel Heterogeneity Experiments Applied to Entire Core

IX. REACTIVITY COEFFICIENTS

The distributed reactivity worths of various materials are required to correct for discrepancies in composition between the Fermi core and its mockup. Further, reactivity worths of fuel and sodium columns are required as a function of radius for safety and kinetics studies and of various materials in local regions as a check on the accuracy of calculations.

A. Distributed Reactivity Worths

A drawer selection was made which gives a good distribution without interfering too much with the core composition. The selection was based on the fact that all core drawers can be included in 27 groups, the drawers of each group having the same radius from the core axis. Hence, all drawers can be represented by 27 drawers of different radii. The sodium column nearest the drawer center was removed from each of these drawers, and the materials of interest were substituted, with the results given in Table XI. Figure 43 shows the arrangement; the nickel reflector

Table XI

DISTRIBUTED REACTIVITY WORTHS

Material	Mass Substituted for Void, kg	Worth of Substitution Relative to Void, Ih	Worth of Material Relative to Void, Ih/kg
Sodium	3.019	41.3	13.7
Stainless Steel	25.77	56.9	2.2
Nickel	34.37	94.6	2.8
Iron	29.97	56.9	1.9
Iron Oxide(1)	9.526	71.7	7.5
Oxygen(2)	-	-	21.7
Physicum I(4)	3.81	-18.9	-2.6
Physicum II	3.36		
0.21% Depleted U	36.24	-43.0	-1.2
93.2% Enriched U	3.017	102.3	33.9
U^{235}(3)	-	-	36.5
U^{238}(3)	-	-	-1.3

(1) Contains 28.5 w/o oxygen and 71.5 w/o iron.

(2) Calculated from experimental worths of the iron and iron oxide.

(3) Calculated from experimental worths of the enriched and depleted uranium.

(4) Compositions for Ph I and Ph II are given in Long et al., "Fast Neutron Power Reactor Studies with ZPR-III," Table 10, Progress in Nuclear Energy, Series II, Vol. 2. The third and fourth columns refer to the mixture.

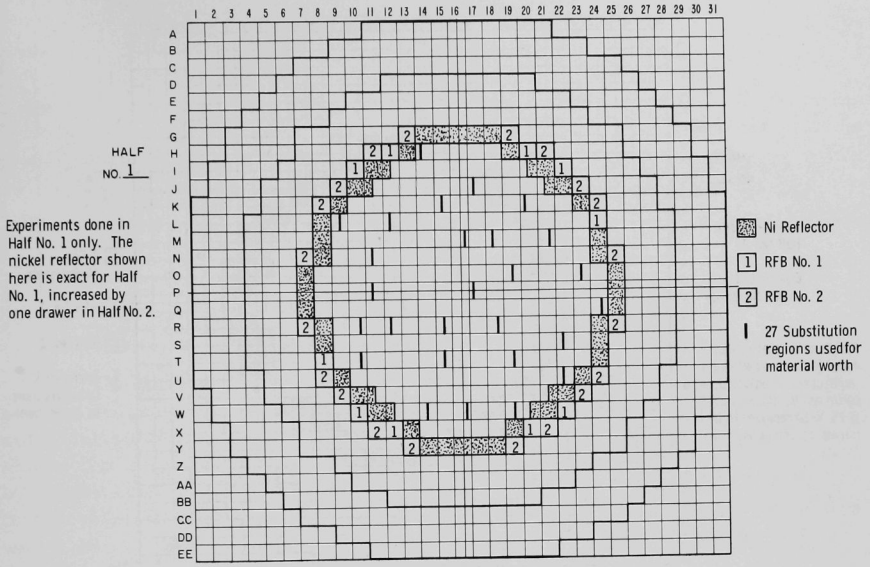

Fig. 43. Assembly Configuration for Distributed Worths Experiments

shown is the nominal reflector which varied within ± 2 drawers for any given experiment. The equivalent reflector thickness, hence, varied between 1.69 and 1.82 in. The distributed worth of fully enriched uranium was measured by first restoring the normal core composition and then inserting columns of fully enriched uranium foils into the center of the 27 drawers of Fig. 43.

B. Radial Worths of Enriched Uranium and Sodium Columns

Figure 44 shows the assembly arrangement used to measure the worth of an 18-in. axial column of fully enriched uranium in a number of radial positions. The measurements were made relative to void (i.e., an air-filled volume), with a nickel reflector of 1.71-in. equivalent thickness. The measurements at the two outer radii were repeated with an increased thickness of nickel reflector in the immediate neighborhood. Figure 44 shows the 15 extra reflector drawers added for these two measurements.

The results of these measurements with uranium columns are given in Table XII and Fig. 45.

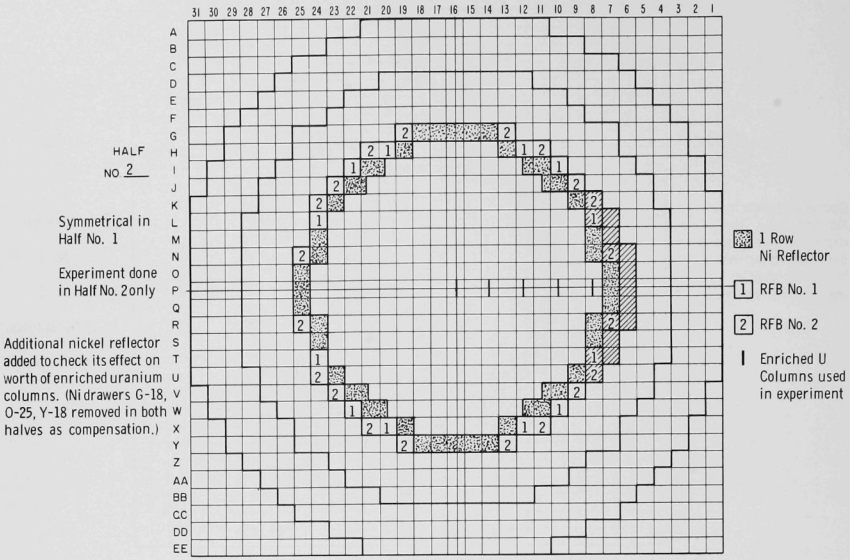

Fig. 44. Assembly Configuration for Measurements of Worth of Enriched Uranium Column

Table XII

WORTH OF ENRICHED URANIUM COLUMN AT VARIOUS RADII

Radius, in.	Mass of Enriched Uranium in Column, kg	Worth of Column Relative to Void		Remarks
		Ih	Ih/kg-Column(1)	
0.03	0.6649	41.1	61.8	
4.40	0.6649	37.6	56.6	
8.67	1.327	60.0	45.2	Symmetrical one-row critical nickel reflector.
13.04	1.327	40.2	30.3	
17.54	1.327	22.6	17.1	
17.54	1.327	24.9	18.8	Second-row nickel reflector added locally.
13.04	1.327	42.6	32.1	Unsymmetrical reflector.

(1) These figures give the worth of 1 kg of enriched uranium distributed along an axial column.

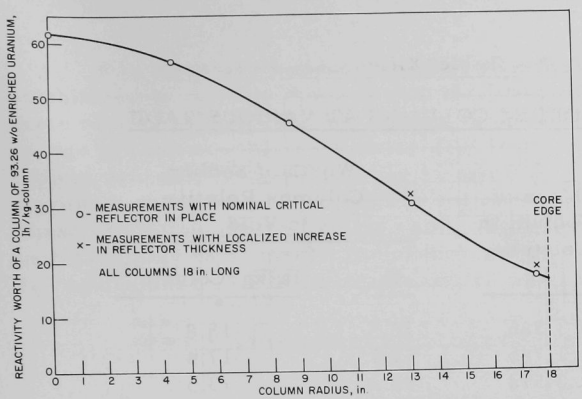

Fig. 45

Reactivity Worth of Enriched Uranium Column Versus Radius

The assembly arrangement used to measure the radial worths of sodium columns is more complicated, because of the increased volume substitution necessary for an appreciable reactivity change. Figure 46 shows the circumferential arrangement of the sodium columns replaced by empty cans at four core radii (18-in.-long columns) and one radius in in the reflector (21-in.-long columns). The equivalent reflector thickness was 1.84 in. The results of these experiments are given in Table XIII and Fig. 47.

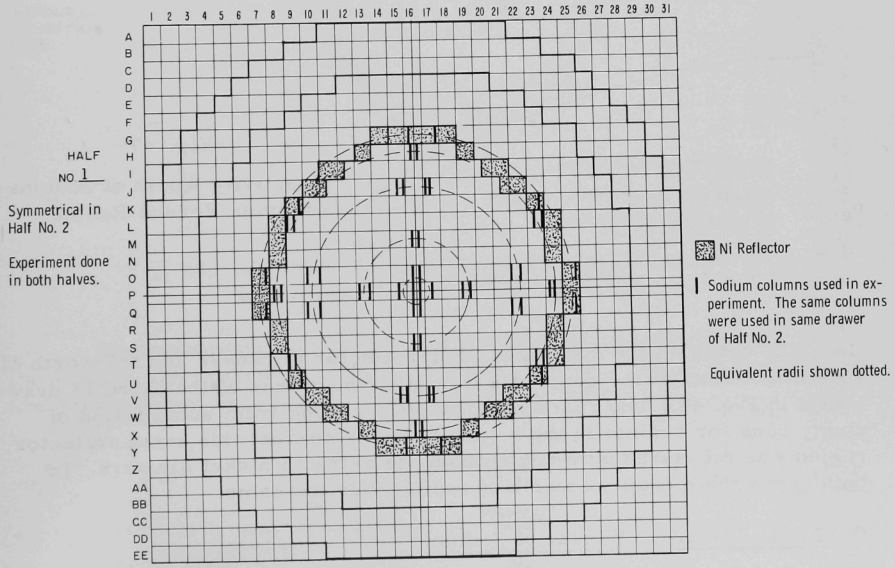

Fig. 46. Assembly Configuration for Measurements of Worth of Sodium Column

Table XIII

WORTHS OF SODIUM COLUMNS AT VARIOUS RADII

Average Column[1] Radius, in.	Mass of Sodium in Columns, kg	Worth of Sodium Columns Relative to Void, Ih	Ih/kg-Column[2]
1.72	1.786	33.5	18.8
6.53	1.786	31.1	17.4
13.11	3.572	48.2	13.5
17.71	3.572	33.7	9.4
19.42	2.679	17.9	6.7

(1) "Column" here refers to a column half-way between the two substitution columns in each core drawer, and to the single substitution column in each nickel-reflector drawer (radius of 19.42 in.).

(2) These figures give the worth of 1 kg of sodium distributed along an axial column.

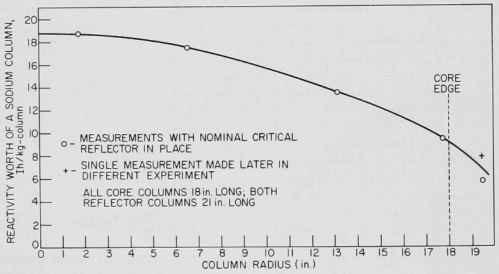

Fig. 47

Reactivity Worth of Sodium Columns Versus Radius

A check on the effect of nickel-reflector thickness and the worth of sodium columns at the core edge was made by means of the extra 15 drawers shown in Fig. 44. The reactivity change resulting from substitution of empty cans for sodium in the 9 core drawers nearest this extra reflector region was measured with and without the extra 15 nickel drawers. In both cases the measured worth of sodium was the same.

C. Local Reactivity Worths of Sodium

Since this was the first large assembly where no substitute was used (in core and fine blankets) to mock up sodium, a fairly thorough investigation of the local reactivity worths of sodium was possible and desirable.

For these worth measurements, nine different local volumes were established by dividing the core into three axial zones in each of the three radial regions. The limitations on the experiments were a minimum change of sodium volume for acceptable reactivity change, a maximum sodium volume consistent with the localization of the volumes, and the maximum change of sodium volume set by the supply of empty cans. These limitations restricted the axial length of each volume to 4 in. in each assembly half, and the radial distribution to that shown in Fig. 48. The equivalent nickel-reflector thickness was 1.82 in.

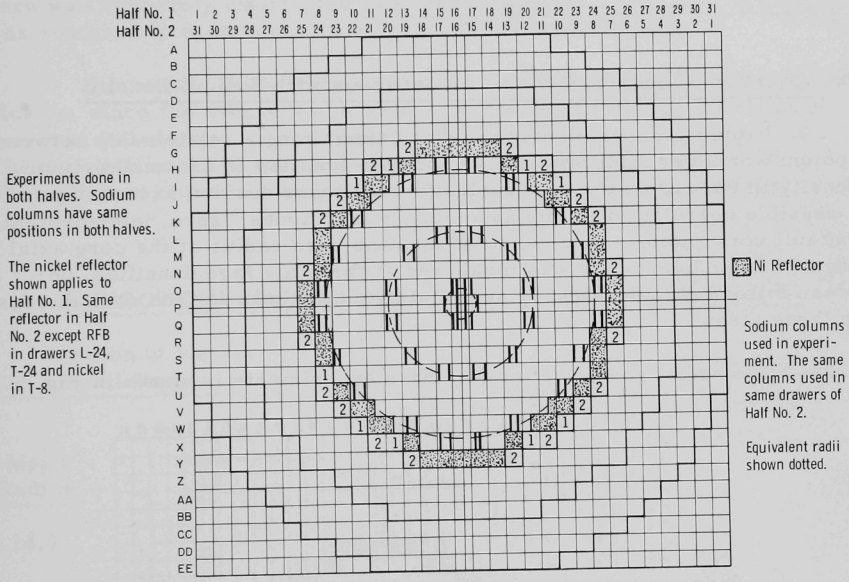

Fig. 48. Assembly Configuration for Measurements of Local Sodium Worth

Measurements were made of sodium worth relative to void, and the results are presented in Table XIV and Fig. 49. The curves of Fig. 49 are shown dotted because of the uncertainty in their shape.

Table XIV

LOCAL REACTIVITY WORTHS OF SODIUM

Position of Experimental Region, in.		Mass of Sodium Removed, kg	Sodium Worth Relative to Void,	
Average Column Radius	Mean Distance from Central Plane		Ih	Ih/kg
17.06	2	1.854	23.7	12.8
	9	1.854	19.5	10.5
	16	1.854	10.9	5.9
9.07	2	1.051	20.2	19.2
	9	1.173	17.0	14.5
	16	1.173	11.0	9.3
2.10	2	0.5866	11.7	19.9
	9	0.5866	11.3	19.3
	16	0.5866	8.9	15.2

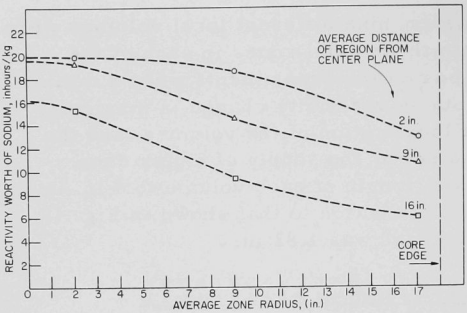

Fig. 49

Reactivity Worth of Sodium in Local Volumes

D. Variation of Sodium Reactivity Coefficient with Sodium Density

Previous experiments aimed at determining a relationship between sodium worth per kilogram in a region as a function of the total sodium density in the region were inconclusive.[5] It was decided to investigate a possible correlation in this assembly in four zones: zero, intermediate, and full core radius at the center plane, and zero radius at the core axial edge. The sodium worth was measured at three average densities, between full and zero density, by substituting empty cans for the sodium cans in three steps.

The radial configuration for these experiments is shown in Fig. 50.

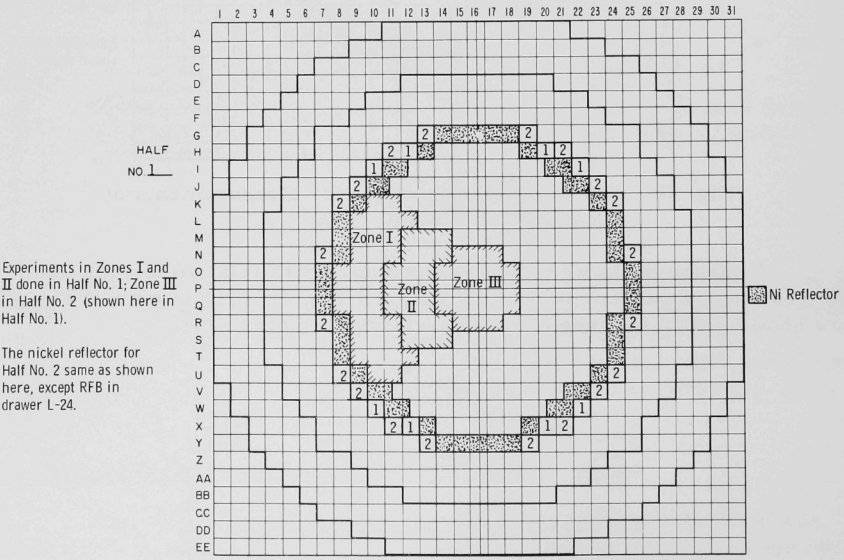

Fig. 50. Outline of Core Zones for Sodium Density-worth Experiments

A limited segment was necessary so the supply of empty cans would be sufficient to reduce the sodium density to zero. Each zone was 6 in. in axial length, i.e., lay between 0 and 6 in. from the center plane for the three radial zones, and between 0 and 6 in. from the core-axial blanket interface for the fourth zone. This latter zone has the same radial configuration as the inner zone in Fig. 50. The equivalent nickel-reflector thickness was 1.87 in.

Each of the three steps in the reduction of the sodium density to zero was uniformly distributed throughout the zone. Full sodium density was restored to each zone before proceeding to the next one.

The results of the experiment, presented in Table XV, were inconclusive, since the difference in sodium worth per kg measured between zero and full-density varied between 2% and 9%, depending on the zone. The possible error in each measurement lay, however, between 4% and 8%, so the measured variation could be due entirely to experimental error.

Table XV

EFFECT OF SODIUM DENSITY ON ITS REACTIVITY WORTH

Position of Experimental Region, in.		Sodium Density Reduction, g/cc		Sodium Worth Relative to Void	
Mean Radius	Mean Axial Distance from Midplane	From	To	Ih*	Ih/kg
14.9	3	0.2906	0.1852	-22.6	13.9
		0.1852	0.1058	-17.7	14.5
		0.1058	0	-24.0	14.7
8.8	3	0.2960	0.1880	-20.8	19.8
		0.1880	0.1090	-14.8	18.8
		0.1090	0	-19.3	18.2
3.7	3	0.2999	0.1997	-19.3	19.6
		0.1997	0.1000	-20.1	20.6
		0.1000	0	-18.6	19.0
3.7	15	0.2999	0.1997	-15.1	15.3
		0.1997	0.0999	-15.0	15.3
		0.0999	0	-15.3	15.6

*Estimated accuracy ± 1 Ih.

E. Local Reactivity Worths

Measurements of local reactivity coefficients for various materials were made in general at the midplane at three radii: core center, core edge, and an intermediate radius. Additional measurements were made with plutonium at the inner edge of the radial blanket at the center plane, and of depleted uranium at two axial positions in the core.

The fissile materials at each radius were inserted into a $\frac{1}{8}$-in. substitution region located at the front of the drawers shown in Fig. 51 in both halves of the reactor. For the nonfissile materials in general, the substitution region was increased to 1 in. The nickel reflector had an equivalent thickness of 1.75 in. for all measurements made at core edge, at core center for the materials with positive reactivity worth, at blanket inner edge for plutonium, and on axis for depleted uranium. It was increased to 1.80 in. for all measurements at the intermediate radius and to 1.87 in. for measurements with materials of negative worth at the core center.

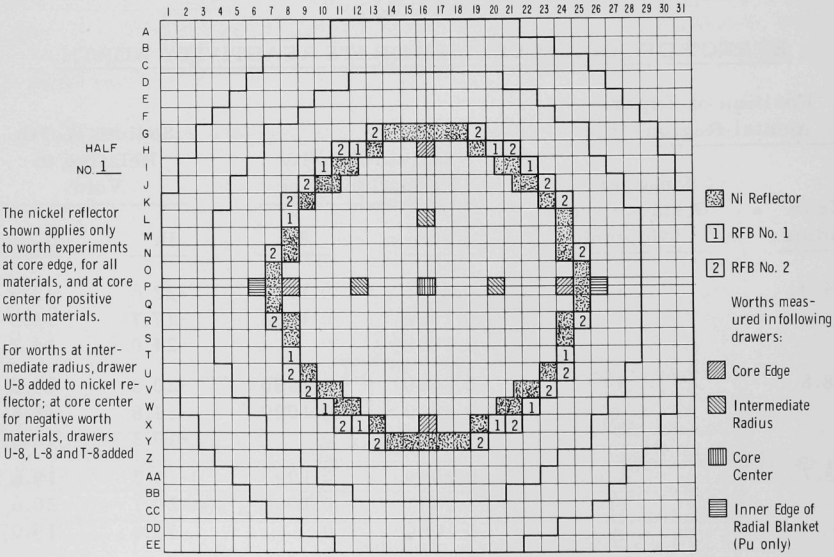

Fig. 51. Assembly Configuration for Local Reactivity Worth Measurements

The results of all the local worth measurements are given in Table XVI.

Table XVI

LOCAL REACTIVITY WORTHS OF MATERIALS

Position of Material from Core Center, in.			Reactivity Worth Relative to Void	
Radial	Axial	Material	Ih	Ih/kg
17.44	0	Stainless Steel	6.13	3.0
		Nickel	7.21	3.2
		Enriched Boron(1)	-21.82	-702
		Depleted Uranium(2)	-0.45	-0.09
		Enriched Uranium(3)	29.83	25.9
		Plutonium(4)	21.28	38.7
		U^{235}(9)	-	27.8
		U^{238}(9)	-	-0.15
8.72	0	Stainless Steel	4.40	2.16
		Nickel	5.02	2.22
		Enriched Boron(1)	-28.70	-1851
		Depleted Uranium(2)	-14.49	-3.0
		Enriched Uranium(3)	37.69	65.4
		U^{235}(9)	-	70.38
		U^{238}(9)	-	-3.2
0	0	Stainless Steel(10)	1.04	1.0
		Nickel(10)	0.47	0.4
		Iron(10)	0.94	0.9
		Iron Oxide(5)	7.32	11.7
		Sodium	2.00	22
		Chromium	1.12	2.5
		Aluminum	4.16	11.9
0	0	Aluminum Oxide(6)	8.51	23.9
		Carbon	14.22	69.8
		Beryllium	33.83	140.5
		Oxygen(11)	-	38.8
		Oxygen(12)	-	37.5
0	0	Plutonium(4)	21.14	153.9
		Enriched Uranium(3)	25.63	88.9
		Physicum I(7)	-2.87	-12.4
		Physicum II(7)	-2.52	-12.00
		Enriched Boron(1)	-18.78	-2538
		Natural Boron Carbide(8)	-19.86	-343.5
		Depleted Uranium(2)	-13.10	-5.4
		U^{235}(9)	-	95.8
		U^{238}(9)	-	-5.6
0	9	Depleted Uranium(2)	-4.74	-2.7
0	16	Depleted Uranium(2)	+0.31	+0.2
19.62	0	Plutonium(4)	9.08	16.5

(1)94 w/o B, 92 a/o B^{10}, 6 w/o impurities.
(2)0.21% depleted uranium.
(3)93.2% enriched uranium.
(4)94.51 ± 0.08 a/o Pu^{239}, 5.11 ± 0.07 a/o Pu^{240}, 0.38 ± 0.03 a/o Pu^{241}.
(5)28.5 w/o O, 71.5 w/o Fe (including impurities).
(6)47.1 w/o O, 52.9 w/o Al.
(7)For composition, see Table XI.
(8)77 w/o B, 19.2 a/o B^{10}, 23 w/o C.
(9)By calculation from enriched and depleted uranium.
(10)These experiments were repeated at a later date because of surprising results for nickel. The results were the same.
(11)By calculation from iron and iron oxide.
(12)By calculation from aluminum and aluminum oxide.

F. Radial and Axial Traverses of Fissionable Materials

Small samples of enriched and natural uranium were traversed through the assembly to obtain the variations in their worths as a function of radial and axial position.

1. Traverses along Core Axis

The central-core and axial-blanket drawers in each assembly half (drawers 1- and 2-P-16) were modified to allow insertion of a $\frac{1}{2}$-in.-diameter aluminum guide tube along the reactor axis. (In the core sections the $\frac{1}{8}$-in. enriched uranium columns were replaced by two $\frac{1}{16}$-in. columns at the drawer edges.) A $\frac{3}{8}$ x $\frac{1}{2}$-in.-long enriched uranium cylinder was guided remotely through the tube, and control-rod critical positions were established for a number of axial positions of the sample. The enriched uranium sample was replaced by a $\frac{3}{8}$ x 2-in. natural uranium sample and the traverse repeated. A traverse was also run with no sample connected to the tip of the guide rod (a "blank" run), and the uranium sample worths for each axial setting were determined from the difference in control-rod critical positions, corresponding to that setting, with the samples and without (blank). During these runs the equivalent thickness of the nickel radial reflector was 1.81 in.

The measured worths, in Ih/kg, of enriched (93.1%) and natural uranium as a function of axial position are presented in Table XVII. These results are also plotted in Figs. 52 and 53. Comparison of the enriched uranium worth at the core center in Table XVII with the central reactivity worth in Table XVI reveals a -3.1% difference, which most likely is due to the limited experimental accuracy of the traverse measurements.

2. Traverses at Core Radial Edge Parallel to Axis

In a manner similar to the traverses along the core axis, the uranium samples were run through drawers 1- and 2-H-16 at the core radial edge. Here, the guide tube was parallel to the reactor axis at a radius of 17.4 in. During these traverses the radial nickel-reflector thickness was 1.81 in.; however, the reflector immediately adjacent to the traverse drawers was 2.18 in. thick.

The uranium worths, as a function of distance from the interface, are given in Table XVII along with the axial data. The enriched uranium results are plotted in Fig. 52.

Table XVII

AXIAL TRAVERSES OF URANIUM REACTIVITY SAMPLES

Axial Position, in. from Midplane	Traverses along Assembly Axis (in P-16, Radius = 0.0 in.)		Traverses at Core Radial Edge Parallel to Axis (in H-16, Radius = 17.4 in.)	
	Worth Enriched Uranium,(1) Ih/kg (± 2.5)	Worth Natural Uranium,(2) Ih/kg (± 0.9)	Worth Enriched Uranium,(1) Ih/kg (± 2.5)	Worth Natural Uranium,(2) Ih/kg (± 0.9)
45	0	0	0	0
32	-	-	.8	-
28	2.5	0	.8	-
24	12.4	+0.4	2.1	-
20	20.7	+1.3	2.5	-
18	28.9	+0.7	4.1	+0.6
16.5	37.6	+0.7	6.6	-
15	39.2	+1.6	9.5	-
12	-	-1.6	-	-
9	66.1	-2.2	15.7	-0.9
6	-	-4.4	-	-
3	85.5	-4.4	21.1	-
0	91.7	-3.8	23.1	+0.4
-3	88.4	-4.0	23.5	-
-9	66.1	-4.0	19.0	-
-15	38.4	+1.2	10.7	-
-16.5	36.3	-	-	-
-18	29.3	-	4.1	-

(1)Enriched Uranium = 93.1 w/o U^{235}: Sample size - Cylinder $\frac{7}{16}$ in. dia x $\frac{1}{2}$ in. length. Mass - 22.93 g.

(2)Natural Uranium Sample size - Cylinder $\frac{7}{16}$ in. dia x 2 in. length. Mass - 64.39 g

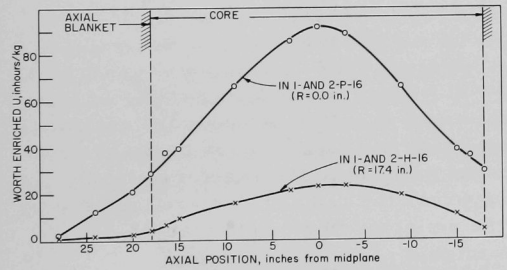

Fig. 52

Axial Traverses of 93.1% Enriched Uranium Sample at Radii = 0 and 17.4 in.

Fig. 53

Axial Traverse of Natural Uranium Sample at Radius = 0 in.

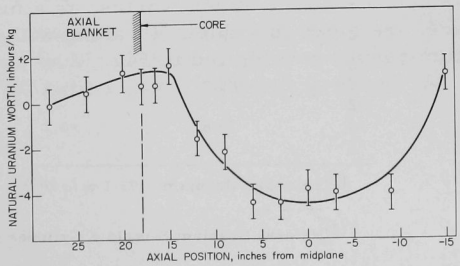

3. Radial Traverses at Midplane with Nickel Reflector

For traversing in a radial direction, the core and blanket drawers in column 16 of Half No. 2 were modified at the front to allow insertion of the guide tube from the top of the matrix through to drawer 2-T-16. Traverses were made with the enriched uranium sample, the natural uranium sample, and the blank. Worths for uranium were thereby found at several radial positions in the core, nickel reflector, and radial blanket. The equivalent nickel-reflector thickness around the core at the time was 1.84 in., but the reflector region through which the traverse was run, 2-G-16 and adjacent drawers, was 2.18 in. thick.

The results of these runs are listed in Table XVIII. The uranium worths versus radii with the nickel reflector are plotted in Figs. 54 and 55.

Table XVIII

RADIAL TRAVERSES OF URANIUM REACTIVITY SAMPLES AT ASSEMBLY MIDPLANE

	Traverses with Nickel Radial Reflector		Traverses with NiO Radial Reflector	
Radius, in.	Worth Enriched Uranium,(1) Ih/kg (± 2.5)	Worth Natural Uranium,(2) Ih/kg (± 0.9)	Worth Enriched Uranium,(1) Ih/kg (± 2.5)	Worth Natural Uranium,(2) Ih/kg (± 0.9)
32.7	0	0	-	-
28.3	-1.2	-	-	-
27.5	-	-	0	0
24.3	-	+0.6	-	-
23.5	-	-	8.3	+1.9
22.9	6.5	-	-	-
20.6	15.7	+0.9	16.6	+1.4
19.6	16.7	-	-	-
18.5	19.6	-0.5	22.7	+0.9
17.5	-	-	26.6	+0.8
17.0	23.1	-	-	-
16.0	26.2	-2.5	34.9	+0.8
14	33.6	-	41.9	-0.5
12	46.2	-2.3	-	-
11	-	-	58.4	-0.8
10	55.4	-	-	-
8	67.1	-2.6	68.5	-2.5
6	74.6	-2.6	-	-
5	-	-	77.2	-3.3
3	78.5	-4.0	-	-
2	-	-	84.6	-4.2
0	83.7	-5.3	81.1	-5.6
-2	-	-	84.2	-5.8
-3	79.8	-5.7	-	-
-5	-	-	76.8	-4.5

(1) Enriched Uranium = 93.1 w/o U^{235} - Cylinder $\frac{7}{16}$ in. dia x $\frac{1}{2}$ in. length. 22.93 g.

(2) Natural Uranium Sample - Cylinder $\frac{7}{16}$ in. dia x 2 in. length. 64.39 g.

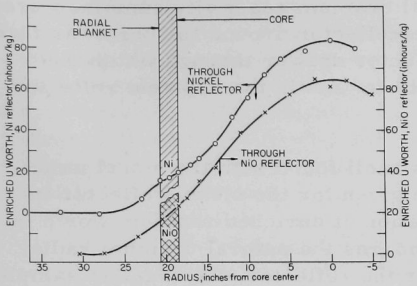

Fig. 54

Radial Traverses of 93.1% Enriched Uranium Sample at Midplane through Ni and NiO Reflectors

Fig. 55

Radial Traverse of Natural Uranium Sample at Midplane through Ni and NiO Reflectors

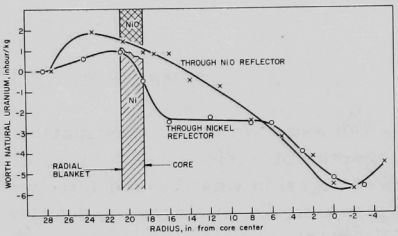

Again a difference was found in the central worth of enriched uranium as found in the traverse measurement from that found in the central reactivity coefficient measurement (see Table XVI), a difference of -5.2 Ih/kg. The measurement of Table XVI was repeated, giving the same value of 88.9 Ih/kg for the central worth of enriched uranium.

If the traverse worth at the radius 17.44 in. is compared with the reactivity coefficient at that position given in Table XVI, a difference of -4 Ih/kg is observed. This suggests an overall error in the enriched uranium traverse results of about 4 to 5 Ih/kg, possibly due to measurements for the worth of the blank traverse. If the enriched uranium traverse results are to be used for obtaining U^{235} worths at local reactor positions, they should probably be first normalized to a central value of 88.9 Ih/kg.

4. Radial Traverses at Midplane with Type "B" Nickel Oxide Reflector

At the conclusion of the Assembly 35 program, the Type "A" nickel radial reflector was replaced by a nickel oxide mockup composition (see Section XI). With this Type "B" nickel oxide reflector in place, the

radial traverses of enriched and natural uranium reactivity samples were repeated. The average thickness of the reflector around the core was then 1.49 in., but in drawer 2-G-16, the reflector drawer through which the traverse was run, the thickness was 2.18 in. and in the adjacent reflector drawers the thickness was 1.47 in.

The uranium worths versus radii found with the nickel oxide reflector are tabulated along with those given for the nickel reflector in Table XVIII. Figure 54 shows the variation of enriched uranium worth in the two reflector cases and Fig. 55 compares the natural uranium radial worths. It is seen that, in the core near the reflector, the uranium samples are more reactive with the nickel oxide composition reflector than with the nickel type.

X. COMPARISON OF REFLECTOR WORTHS

An experimental investigation was made of the comparative reactivity worths of various radial reflector compositions and thicknesses. The investigation was divided into two parts: first, the width of a segment of the usual nickel reflector and one with higher nickel content (Types "A" and "B," respectively) was increased; and second, a segment of the usual nickel reflector was replaced in turn by nickel oxide, iron oxide, beryllium, and beryllium oxide compositions.

Because of the increased reactivity effect expected from most of these substitutions compared with the usual nickel reflector, it was obvious that they would have to be confined to a segment. A substitution of the complete reflector would have been time-consuming and required a corresponding reactivity decrease by fuel removal from the core.

A. Reactivity Effects of Types "A" and "B" Nickel-reflector Thicknesses

Figure 56 shows the segment used for these experiments and the three different rows involved in the increased thickness. Part of Row 2 and all of Row 3 would normally contain radial medium blanket composition. This was first replaced by radial fine blanket composition over the 21-in. drawer length from the central plane (i.e., covering the 18-in. half core length and 3-in. axial fine blanket) to bring it into conformity with the original experiments with the nickel reflector described in Section IV. It will be noticed that Row 1 is slightly thicker than that corresponding to criticality (shown in Fig. 34). The equivalent annular thickness of Row 1 on an area basis is 2.79 in., Row 2 is 2.73 in., and Row 3 is 2.68 in.

The first two rows were built up in steps by substituting Type "A" nickel-reflector drawers of Fig. 23 with 5.443 g/cc nickel, 0.1594 g/cc sodium, and 0.9544 g/cc stainless steel, for radial fine blanket, drawer

types 1 and 2. These steps were paralleled and their reactivity gains compensated by a step-wise removal of Row 1 of the nickel reflector in the diagonally opposite segment of the other reactor half. The resulting distorted reflector shape is not amenable to quotation on an equivalent-area basis, and this should be borne in mind when analyzing the results given in Table XIX and Fig. 57. The reactivity worths quoted are a linear extrapolation of the experimental results for the segment to the full reflector circumference.

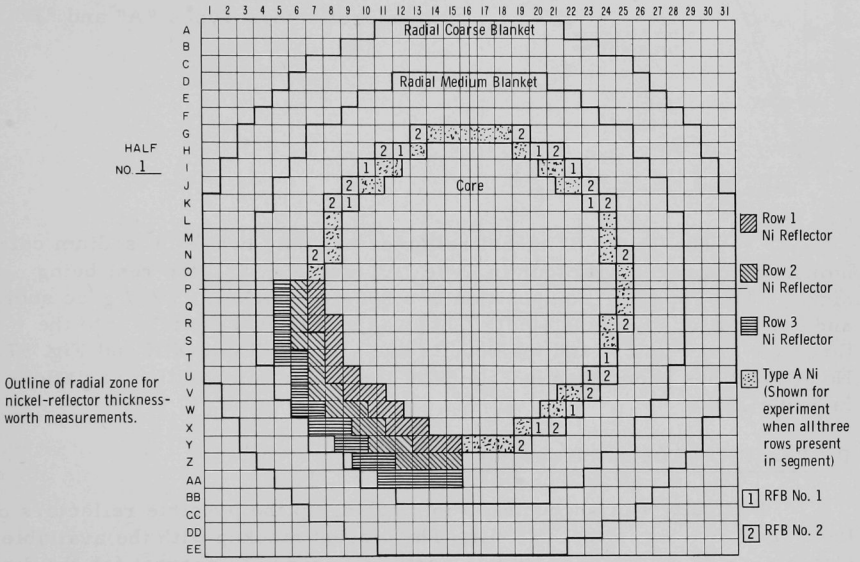

Fig. 56. Outline of Radial Zones for Nickel-reflector Thickness-worth Measurements

Table XIX

NICKEL-REFLECTOR WORTH AS A FUNCTION OF COMPOSITION AND THICKNESS

Row No.	Equivalent Annular Thickness (in.)	Radial Fine Blanket Removed (g/cc)				Nickel Reflector Inserted				Relative Worth of Full Row (1h)
							Composition, (g/cc)			
		Depleted Uranium	Molybdenum	Sodium	Stainless Steel	Type	Nickel	Sodium	Stainless Steel	
Critical[1]	2.01	7.449	0.2243	0.2875	1.391	A[2]	5.421	0.1608	0.9595	1016
1	2.79	7.540	0.2237	0.2762	1.457	A[2]	5.427	0.1604	0.9580	1302
1	2.79	7.540	0.2237	0.2762	1.457	B[2]	6.340	0.0802	0.8359	1455
2	2.73	7.532	0.2233	0.2789	1.425	A	5.443	0.1594	0.9544	468
2	2.73	7.532	0.2233	0.2789	1.425	B	6.350	0.0797	0.8330	475
3	2.68	7.492	0.2233	0.2789	1.444	B	6.350	0.0797	0.8330	133

(1)This is the critical reflector for unseeded control rods. All other results in this table were obtained with the seeded control rods. The reflector worths with seeded and unseeded control rods are comparative, however, as the reflector changes given here do not affect the control rod calibration.

(2)These three reflectors are not precisely Type "A" or "B;" the variation is very small, however, and is neglected in the designation.

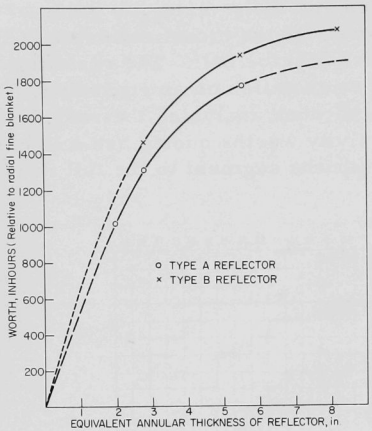

Fig. 57

Reactivity Worth Versus Thickness of Nickel-reflectors Types "A" and "B"

The Type "B" nickel reflector has only two $\frac{1}{8}$-in. sodium columns, as compared with four in Type "A" (see Fig. 23), the rest being nickel. The Type "B" composition is 6.350 g/cc nickel, 0.0797 g/cc sodium, and 0.8330 g/cc stainless steel. This was substituted in steps into the three rows of Fig. 56, and the results are given in Table XIX and Fig. 57. No account has been taken in Fig. 57 of the minor composition variations in Table XIX.

B. Reactivity Effects of Various Reflectors

Difficulty was encountered in mocking up the possible reflectors of the Fermi reactor in the ZPR-III. The closest mockup with the available materials was made and material worths measured to correct for the discrepancy. Table XX gives the composition of the Fermi reflectors, their corresponding ZPR-III mockups, and the discrepancies.

The mockup was again made in a quadrant as shown in Fig. 58. It will be seen that the configuration of this quadrant is almost the same as that of Row 1 in Fig. 56. The only difference is the elimination of the partially loaded drawers containing both core and reflector to expedite the experiment by simplification; it leads to no error since we are interested in comparisons. The equivalent reflector thickness in the quadrant was 2.81 in. The reactivity changes of the various reflectors substituted in this quadrant led to substantial changes in the remaining nickel reflector. The latter will not be quoted, again because of the distorted reflector shape.

Table XX

COMPOSITIONS OF POSSIBLE FERMI REFLECTORS AND THEIR MOCKUPS

Reflector		Composition, g/cc					
		Ni	O	Be	Na	Stainless Steel	Fe
Ni, Type "A"		5.443	-	-	0.1594	0.9544	-
NiO	Fermi	3.22	0.88	-	0.23	1.21	-
	ZPR-III Type "A"	2.722	0.428	-	0.1594	0.9544	1.073
	Discrepancy*	+0.50	+0.45	-	+0.07	+0.26	-1.07
Fe_2O_3	Fermi	-	0.82	-	0.23	1.21	1.92
	ZPR-III	-	0.692	-	0.1594	1.354	1.736
	Discrepancy*	-	+0.13	-	+0.07	-0.14	+0.18
Be	Fermi	-	-	1.01	0.23	1.21	-
	ZPR-III	-	-	1.149	0.1594	0.9544	-
	Discrepancy*	-	-	-0.14	+0.07	+0.26	-
BeO	Fermi	-	1.06	0.60	0.23	1.21	-
	ZPR-III	-	0.428	0.766	0.0797	0.833	1.073
	Discrepancy*	-	+0.63	-0.17	+0.15	+0.38	-1.07

*The positive sign indicates the Fermi composition is greater than ZPR-III.

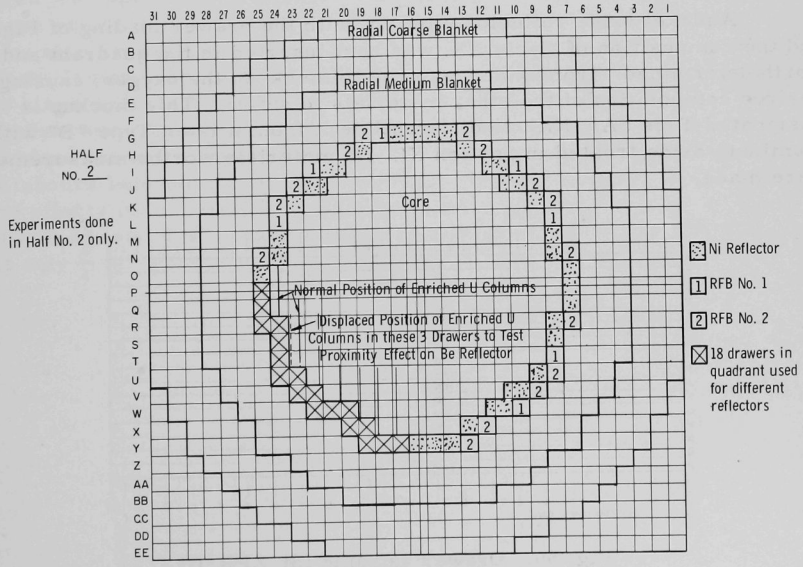

Fig. 58. Assembly Configuration for Experiments with Radial Reflectors of Different Compositions

A reference loading was made with Type "A" nickel reflector in this quadrant. The average worths of various materials were then measured in axial columns at approximately the radial center of all 18 drawers in the quadrant. The results are given in Table XXI.

Table XXI

MATERIAL WORTHS IN THE ZPR-III REFLECTORS

ZPR-III Reflector of Table XX	Average Material Worths Relative to Void in Reflector, Ih/kg								
	Ni	Na	Stainless Steel	Fe	Fe_2O_3(a)	O(b)	Al(c)	Al_2O_3(d)	Be
Type "A" Ni	1.6	7.8	1.5	1.4	3.0	7.0	2.2	5.4	-
Fe_2O_3	2.0	5.7	1.6	1.4	2.9	6.6	-	-	-
Be	1.5	5.1	1.2	1.2	2.6	6.3	-	-	7.0
BeO	-	5.9	1.6	1.5	2.7	5.9	-	-	8.5

(a) Composition: 28.5 w/o O, 71.5 w/o Fe (including impurities).

(b) Calculated from the results for Fe and Fe_2O_3.

(c) Calculated from measured Al_2O_3 and derived O of (b).

(d) Composition: 47.1 w/o O, 52.9 w/o Al.

A nickel oxide reflector mockup, with the drawer loading of Fig. 59 and the composition of Table XX, was next inserted in the quadrant and its worth determined. Iron oxide was used to mock up the oxygen, causing the desired composition of the other materials to suffer. This mockup is designated Type "A," NiO, to differentiate it from a later Type "B" with aluminum oxide treated in Section XI. No materials worths measurements were made.

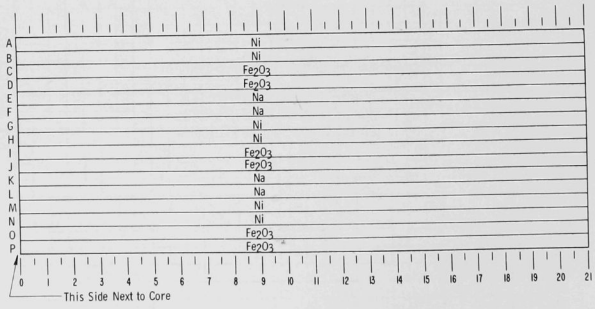

Fig. 59. Drawer Loading for ZPR-III Type "A" NiO Reflector

An iron oxide reflector mockup, with the drawer loading of Fig. 60 and the composition of Table XX, was next inserted in the quadrant and its worth determined. The material worth measurements were repeated in the 18 drawers, giving the results of Table XXI.

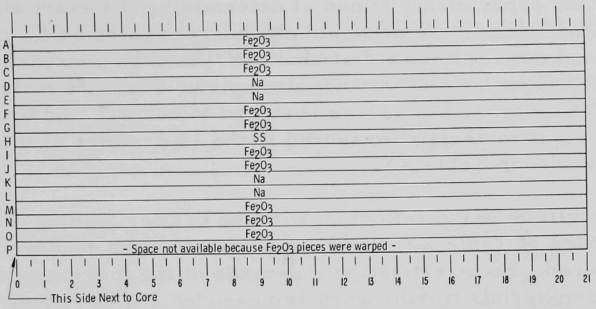

Fig. 60. Drawer Loading for ZPR-III Fe_2O_3 Reflector

Next, a beryllium reflector mockup, with the drawer loading of Fig. 61 and the composition of Table XX, was inserted in two steps in the quadrant, and some surprising results were obtained. The first step involved the upper nine drawers of the quadrant and gave 14.3 inhours increase relative to Type "A" nickel, whereas the second step involved the lower nine drawers and gave 52.2 inhours increase relative to Type "A" nickel. It was suspected that a fuel-proximity effect was responsible for this large difference, since core fuel is in general closer to the lower nine drawers. To test this, nickel reflector was restored to the upper nine drawers and a loss of 18.1 inhours measured. The difference of 3.8 inhours between this and the previous measurement could be due to edge effects in the beryllium reflector. Next, the fuel in core drawers R-23, S-23, and T-23 was moved $1\frac{1}{8}$ in. closer to the nickel reflector, so that only $\frac{1}{4}$ in., approximately, separated it from the core edge. The worth

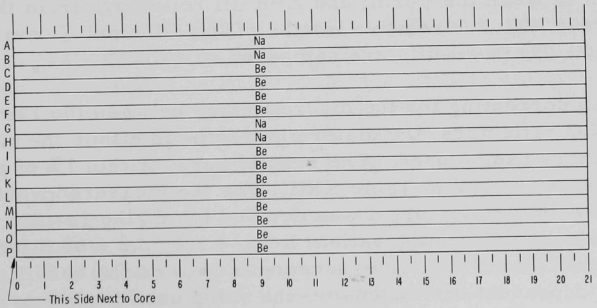

Fig. 61. Drawer Loading for ZPR-III Be Reflector

of beryllium reflector in the upper nine drawers was remeasured and now found to be 41.1 inhours relative to Type "A" nickel. This result, when compared with the previous 18.1 inhours, definitely shows a strong fuel-proximity effect on the worth of a beryllium reflector.

Further experiments aimed at determining the exact effect to be expected in the Fermi reactor would obviously require an exact mockup of the core and edge reflector distributions. Such an approach would be extremely cumbersome and was not attempted. The core material in drawers R-23, S-23, and T-23 was restored to normal, and the average worths of various materials measured in the 18 drawers of the quadrant, giving the results in Table XXI.

A beryllium oxide reflector, with the drawer loading of Fig. 62 and the composition of Table XX, was then inserted in the quadrant and its worth measured. No investigation was made of the fuel-proximity effect. The average materials worths were remeasured and are given in Table XXI.

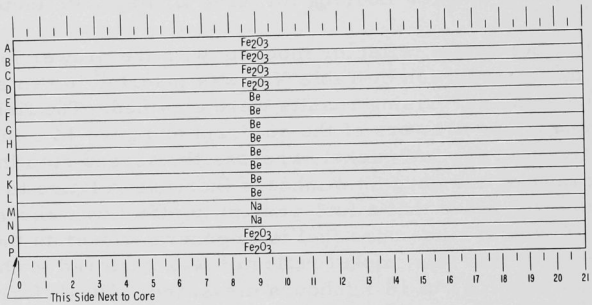

Fig. 62. Drawer Loading for ZPR-III BeO Reflector

By means of the measured reactivity worths of the ZPR-III reflectors relative to Type "A" nickel and corrections for the discrepancies in composition between the Fermi and ZPR-III reflectors from the data in Tables XX and XXI, the relative worths of the different Fermi reflectors can be found. These results are compared in Table XXII.

When correcting for the discrepancies between the Fermi and Type "A" NiO reflectors, the materials worths in either the nickel or iron oxide reflectors can be used. The results agree within 1% of each other, and the average is used in Table XXII. For the measured worth of the ZPR-III beryllium reflector, it was decided to add the results of the steps with normal core fuel configuration, i.e., $14.3 \pm 52.2 = 66.5$ inhours. A further complication is that measurements showed the beryllium worth to be strongly dependent on its density; the value used in the correction for

discrepancies in materials was that for the average beryllium density between the Fermi and ZPR-III beryllium reflectors. The same procedure was adopted for the correction in the beryllium oxide reflector.

Table XXII

COMPARISON OF WORTHS OF VARIOUS REFLECTORS IN ONE QUADRANT OF ONE ASSEMBLY HALF

Note: The compositions for the first column are given in Table XX. The second, third, and fourth columns apply only to the 18 drawers of the quadrant. The fifth column applies to the quadrant, and also to a linear extrapolation of the quadrant to the full core, giving a 2.81-in.-thick reflector.

Fermi Reflector of Table XX	Measured Worth of ZPR-III Reflector Relative to Type "A" Ni, Ih	Calculated Worth of Fermi Relative to ZPR-III Reflector, Ih	Worth of Fermi Reflector Relative to Type "A" Ni, Ih	Worth Ratio, Fermi Reflector / Type "A" Ni Both Relative to RFB
NiO	6.5	97.5	104	1.63
Fe_2O_3	-49.0	38.0	-11.0	0.933
Be	66.5	-6.5	60.0	1.37
BeO	42.7	65.7	108.4	1.66

From Table XXII it is seen that the Fermi beryllium oxide and nickel oxide reflectors gave the greatest reactivity gains. Some doubt exists, though, as to the validity of extrapolation of the measured worth of the BeO reflector to the Fermi reactor, because of the fuel-proximity effect on the worth of beryllium. It was, therefore, decided that the nickel oxide reflector would be the most advantageous one for the Fermi reactor, and that a complete substitution of its mockup for the normal nickel reflector with the repetition of some important experiments would be necessary. These experiments are covered in Section XI.

XI. THE CRITICAL TYPE "B" NiO REFLECTOR

Table XXII shows the Fermi nickel oxide reflector to be 1.63 times as reactive as the Type "A" Ni reflector used for most experiments with this assembly. It will also be noted from this table that approximately 94% of this increase comes from the calculated reactivity difference between the Fermi, NiO, and ZPR-III, Type "A" NiO reflectors, with only 6% resulting from the measured worth of the latter relative to Type "A" nickel. Mocking up this Type "A" NiO, therefore, would show little reactivity difference compared with the normal Type "A" nickel. A more reactive nickel oxide mockup is possible if the sodium and iron oxide of the Type "A," NiO reflector are replaced by aluminum oxide; the aluminum would mock up the sodium. Such a composition is shown by the drawer loading of Fig. 63 and is designated Type "B," NiO. It was calculated that

approximately 75% of the Type "A" nickel-reflector thickness would be required for a critical Type "B" NiO reflector. Hence, the partial drawer loadings of Fig. 63 were used, the nickel oxide composition being turned around in all drawers so that it was nearest core material. The outer part of the drawer contains radial fine blanket composition. The composition of the reflector part of the drawer is 2.700 g/cc nickel, 0.6331 g/cc oxygen, 0.7117 g/cc aluminum, and 0.6118 g/cc stainless steel; the oxygen is seen to have increased by about 50% over that in the Type "A" NiO.

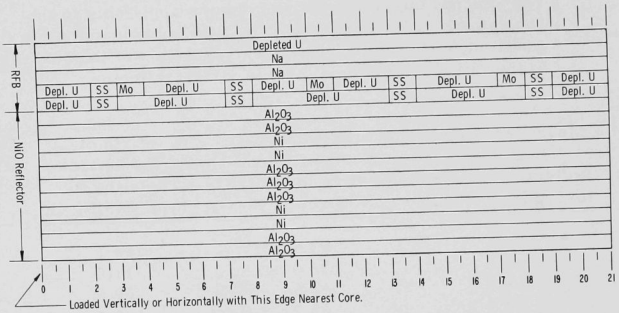

Fig. 63. Nickel Oxide Reflector Drawer, Type "B"

Starting with the complete Type "A" nickel reflector, it was replaced in steps by the Type "B" NiO, giving finally the critical configuration of Fig. 64. A check on the calibration of the operating control rod was then made and found to be insignificantly different from that of the Type "A" reflector. The reflector of Fig. 64 has an equivalent annular thickness of 1.40 in., and the assembly was 23.5 inhours supercritical with all rods in. A measure of the average worth of this reflector gave 8.6 inhours per drawer relative to the radial fine blanket. Consequently, the critical reflector with all rods inserted would have an equivalent annular thickness of 1.32 in. on the core diameter of 35.94 in. This, however, is for the core with seeded control rods, i.e., the core contained 459.39 kg U^{235} compared with the 456.95 kg U^{235} of the uniform composition in Table IV. The reactivity difference between these two cores is 106 inhours (this value is the same with Ni and NiO reflectors since the control rod calibration did not change), so that the critical Type "B" NiO reflector on the core with unseeded control rods would have an equivalent annular width of 1.65 in. This compares with the 2.01-in. value for the Type "A" Ni reflector (see Section III).

This critical nickel reflector with unseeded control rods was found to have a worth of 1016 inhours. Hence, the present critical Type "B" NiO reflector of 1.32-in. equivalent width must have a worth of 1016 - 106 = 910 inhours, since the control rods were seeded. Figure 57 shows that a

1.32-in., Type "A," nickel reflector has a worth of 710 inhours. Therefore, the Type "B" NiO reflector is 910/710 = 1.28 times as reactive as the Type "A" nickel, where both have a thickness of 1.32 in. and replace radial fine blanket.

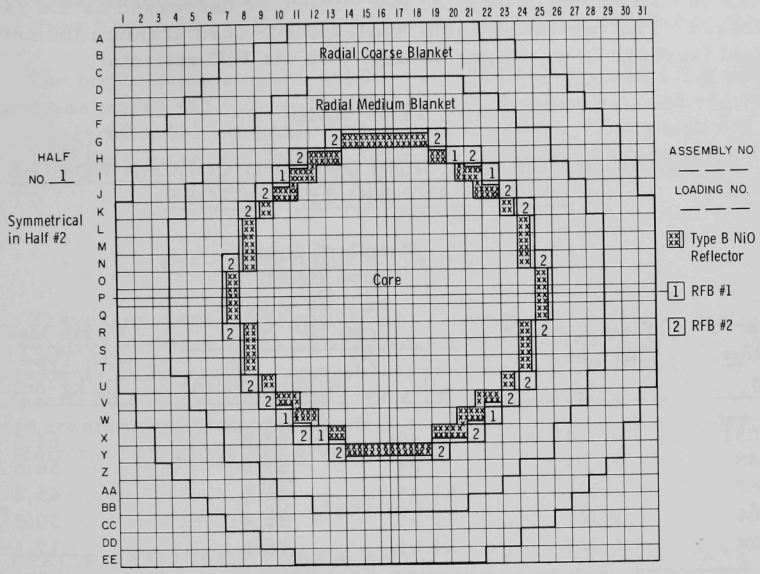

Fig. 64. Interface View of Assembly with 599-liter Core and Critical Type "B" Nickel-Oxide Reflector

Measurements of average materials worths were also made with this reflector, allowing a correction to be applied for the discrepancies between the Fermi and Type "B" NiO compositions. The following worths were obtained in inhours/kg: nickel, 1.8; oxygen, 6.7; aluminum, 3.9; sodium, 5.8; and stainless steel, 1.6, all relative to void. These figures give a correction of 189 inhours, the Fermi reflector being more reactive. Hence, the Fermi NiO reflector is (910 + 189)/710 = 1.55 times as reactive as the Type "A" nickel reflector. In Table XXII this ratio was found to be 1.63, with a distorted Type "A," NiO mockup in a 2.8-in.-thick quadrant.

The radial worth measurements of enriched uranium and sodium columns, described in Section IX, B for the nickel-reflected assembly, were now exactly repeated with the Type "B" NiO reflector. The equivalent thickness of NiO reflector was changed from 1.40 to 1.39 in. for the uranium column experiments and to 1.54 in. for the sodium column experiments.

The results are presented in Tables XXIII and XXIV, which are to be compared with Tables XII and XIII, respectively. The main results from the nickel-reflected assembly are also given in Tables XXIII and XXIV. Only three of the five sodium column radii were repeated, since the difference in sodium worth with the two reflectors decreased as the radius decreased. The results of Table XXIII for enriched uranium indicate only a slight increase in worth per column with the NiO reflector.

Table XXIII

COMPARISON OF ENRICHED URANIUM COLUMN WORTHS WITH Ni AND NiO REFLECTORS

Column Radius, in.	Mass of 93.2% Enriched U, kg	Worth of Substitution Relative to Void with Type "B" NiO		Worth Measured with Type "A" Ni Ih/kg-column*
		Ih	Ih/kg-column*	
0.031	0.6649	41.40	62.3	61.8
4.40	0.6649	37.89	57.0	56.6
8.67	1.327	61.44	46.3	45.2
13.04	1.327	41.59	31.4	30.3
17.54	1.327	24.04	18.1	17.1

*These values refer to 1 kg of 93.2% enriched uranium distributed axially along an 18-in. column.

Table XXIV

COMPARISON OF SODIUM COLUMN WORTHS WITH Ni AND NiO REFLECTORS

Equivalent Columns Radius in.	Mass of Sodium kg	Worth of Substitution Relative to Void with Type "B" NiO		Worth Measured with Type "A" Ni Ih/kg-column*
		Ih	Ih/kg-column*	
6.53	1.786	30.46	17.1	17.4
13.11	3.572	46.41	13.0	13.5
17.71	3.572	31.30	8.8	9.4

*These values refer to 1 kg of sodium distributed axially along an 18-in. column.

The worth of an axial column of enriched boron was also measured as a check on the worth of the safety rod. The column was 16 in. long, i.e., 2 in. short of the core half-height, and was placed in drawer P-20 at a radius of 8.1 in. The equivalent thickness of the NiO reflector was 1.54 in. for this experiment. An exactly similar experiment was performed with the normal Type "A" nickel reflector of 1.78-in. equivalent annular thickness.

The boron column contained 26.7 g B^{10}, 2.6 g B^{11}, and 1.9 g impurities, and was worth -43.6 Ih in the NiO-reflected assembly, and -42.7 Ih in the nickel-reflected assembly both relative to void. The reactivity effect of B^{10} thus increased by approximately 2.1% at the safety rod location.

XII. REACTION RATE TRAVERSES

Traverses were made with fission chambers and $B^{10}F_3$ counters to obtain relative reaction rates as a function of radial and axial positions. Arrangements of the traversing mechanism were the same as for the uranium reactivity sample traverses (see Section IX, F). Enriched uranium, depleted uranium, and plutonium fission chambers, and a $B^{10}F_3$ counter were used; their specifications are given in Table XXV.

Table XXV

SPECIFICATIONS OF FISSION AND $B^{10}F_3$ TRAVERSE COUNTERS

Counter Number	Loading Material	Reactive Mass	Analysis	Active Length, in.
J	Enriched Uranium	5.1 mg	93.2 w/o U^{235}; 6 w/o U^{238}; 1 w/o U^{234}	2
IC-24-1	Depleted Uranium		80 ppm U^{235}	2
T	Pu^{239}	1.96 mg	94.92 w/o Pu^{239}; 4.75 w/o Pu^{240}; 0.315 w/o Pu^{241}; 0.01 w/o Pu^{242}	2
G-15758	$B^{10}F_3$			$2\frac{1}{4}$

During a traverse, count rates were established at several counter positions relative to a standard count on a U^{235} absolute fission chamber at a fixed location near the core edge.

A. Traverses along Assembly Axis

Each of the four counters listed in Table XXV were run through the guide tube in drawers 1- and 2-P-16. At that time, the reactor radial reflector was the Type "A," nickel reflector and the equivalent thickness was 1.81 in. The data of these four runs are presented in Table XXVI, and the relative reaction rates, presented as percent of reaction rates at the core center, are plotted in Fig. 65 for enriched and depleted uranium and in Fig. 66 for B^{10} and Pu^{239}.

Table XXVI

AXIAL COUNTER TRAVERSES THROUGH 1- AND 2-P-16 (Radius = 0 in.)

	Average Chamber Counts per 10^3 Counts on Standard			
Axial Position Z (in.)	Enriched Uranium, #J(a)	Depleted Uranium, #IC-24-1(b)	Pu^{239}, #T(a)	BF_3, #15758(b)
32	251	.9	87	2267
24	1586	13.8	466	8105
20	2963	53.5	856	14245
18	3815	110.2	1111	17997
17	4249	150.0	1313	19531
16	4672	191.5	1466	22355
15	5189	220.1	-	23223
14	5365	239.9	1630	24753
13	5948	-	-	-
12	6208	274.4	1930	28601
8	7318	349.9	2222	33228
6	7694	367.1	2348	34481
4	8132	374.8	2436	35985
3	8110	385.4	2459	37074
2	8246	387.1	2569	36685
1	8304	396.7	2529	36648
0	8293	382.2	2566	37093
-1	8390	392.2	2559	36695
-2	8131	389.0	2540	36546
-3	8295	-	2471	-
-4	8052	377.8	2516	36614
-6	7839	-	2372	-
-8	7308	351.0	2328	33310
-12	6183	-	1982	-
-14	5560	-	1682	-

(a)Rate obtained using standard count of 5×10^3.

(b)Rate obtained using standard count of 2×10^4.

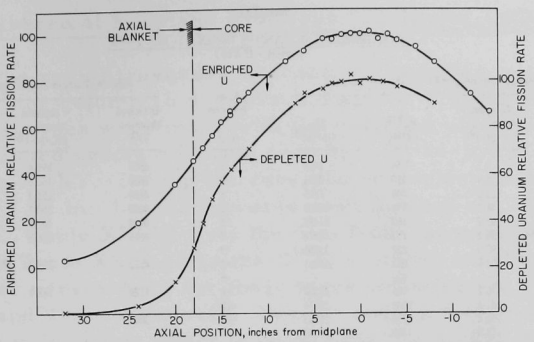

Fig. 65. Axial Traverses of Enriched Uranium and Depleted Uranium Fission Counters in 1- and 2-P-16 (Radius = 0 in.)

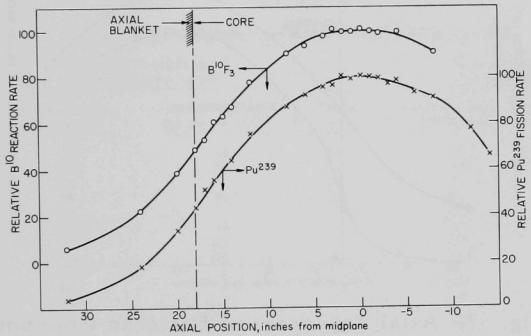

Fig. 66. Axial Traverses of $B^{10}F_3$ and Pu^{239} Counters in 1- and 2-P-16 (Radius = 0 in.)

B. Traverses at Core Radial Edge Parallel to Axis

Traverses were made with the four counters of Table XXV parallel to the axis at a radius of 17.4 in. (through 1- and 2-H-16). Again, the radial reflector was Type "A" nickel, with an equivalent thickness of 1.81 in., but near the traverse the nickel thickness was 2.18 in. The results of these traverses are given in Table XXVII and plotted in Figs. 67 and 68.

Table XXVII

AXIAL TRAVERSES OF COUNTERS THROUGH 1- AND 2-H-16
(Radius = 17.4 in.)

Axial Position Z (in.)	Average Chamber Counts per 10^3 Counts on Standard: Enriched Uranium, #J[a]	Depleted Uranium, #IC-24-1[b]	Pu^{239}, #T[a]	BF_3, #15758[c]	Axial Position Z (in.)	Average Chamber Counts per 10^3 Counts on Standard: Enriched Uranium, #J[a]	Depleted Uranium, #IC-24-1[b]	Pu^{239}, #T[a]	BF_3, #15758[c]
32	144	0.5	59	1428	3	4555	159.4	1291	22794
24	818	5.9	218	3751	2	4620	160.6	1329	22909
20	1658	20.6	448	7705	1	4689	158.3	1337	23266
18	2162	48.3	596	10208	0	4684	160.1	1352	23754
17	2381	65.2	662	11498	-1	4633	161.5	1321	23558
16	2591	83.1	753	12578	-2	4676	158.8	1337	24190
15	2810	92.6	822	13895	-3	-	-	1328	23128
14	2960	100.4	881	14861	-4	4522	158.2	1308	23238
13	3244	-	922	-	-6	-	-	1225	22179
12	-	116.2	996	17004	-8	4120	145.9	1211	20750
8	4021	141.4	1148	20376	-12	-	-	1026	17725
6	4238	150.4	1230	21603	-14	3093	-	877	15075
4	4476	157.4	1262	22780					

(a) Rate obtained using standard count of 1×10^4.
(b) Rate obtained using standard count of 4×10^4.
(c) Rate obtained using standard count of 5×10^3.

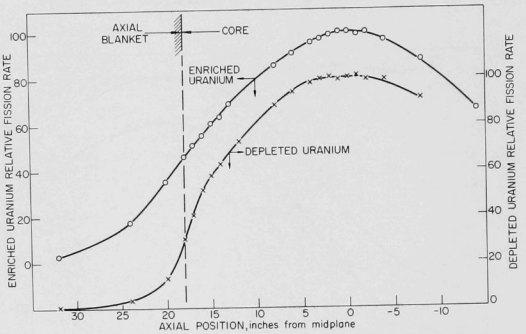

Fig. 67. Axial Traverses of Enriched Uranium and Depleted Uranium Fission Counters in 1- and 2-H-16 (Radius = 17.4 in.)

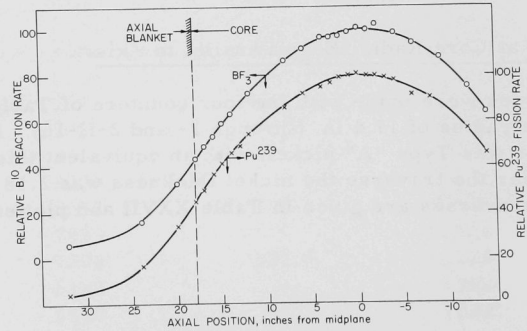

Fig. 68. Axial Traverses of $B^{10}F_3$ and Pu^{239} Counters in 1- and 2-H-16 (Radius = 17.4 in.)

C. Radial Traverse at Midplane with Type "A" Nickel Reflector

As in the radial traverses of reactivity samples, a guide tube was placed through the column 16 drawers in Half No. 2 about $\frac{5}{8}$ in. from the interface. Traverses were made with the enriched uranium fission chamber, J, the depleted uranium fission chamber, IC-24-1, and the $B^{10}F_3$ counter of Table XXV. During the runs, the equivalent nickel-reflector thickness was 1.75 in., but the traverse went through a 2.18-in.-thick reflector region. Table XXVIII lists the data from the enriched and depleted traverses, and Table XXIX gives the $B^{10}F_3$ chamber count rates. The relative count rates versus radii for these three counters are plotted in Figs. 69, 70, and 71, respectively. For the enriched uranium and $B^{10}F_3$ runs, a strong moderating effect is noted near the nickel reflector and also near the blanket outer boundary. The latter effect is probably due to backscattering from polyethylene surrounding ionization chambers on top of the ZPR-III machine or from room walls.

Table XXVIII

RADIAL FISSION RATE TRAVERSES AT CORE MIDPLANE WITH NICKEL REFLECTOR

Radial Position (in.)	Average Chamber Counts per 10^3 Counts on Standard Chamber: Enriched Uranium, Chamber #J[a]	Depleted Uranium, Chamber #IC-24-1[b]	Radial Position (in.)	Average Chamber Counts per 10^3 Counts on Standard Chamber: Enriched Uranium, Chamber #J[a]	Depleted Uranium, Chamber #IC-24-1[b]
33.75	720	1.8	14.0	6888	300.0
33.5	704	1.1	12.0	7522	320.4
33.0	651	-	10.0	8228	361.8
30.5	586	2.6	8.0	8834	395.2
29.0	730	-	6.0	9254	424.9
27.5	948	5.4	4.0	9664	453.2
24.5	1850	14.5	2.0	9994	446.2
21.5	3529	40.3	1.0	9931	438.2
20.5	4635	-	0	9992	451.2
19.5	5666	-	-1.0	10005	439.6
18.5	5986	143.2	-2.0	10075	434.4
18.0	5930	169.2	-3.0	9980	433.3
17.0	6035	-	-4.0	9629	424.9
16.0	6251	232.8	-5.0	9256	419.8

[a] Rate obtained using standard count of 1 x 10^4.

[b] Rate obtained using traverse count of 1 x 10^4.

Table XXIX

RADIAL TRAVERSE OF BF_3 COUNTER AT CORE MIDPLANE WITH NICKEL REFLECTOR

Radial Position (in.)	Average BF_3 Counts per 100 Counts on Standard[1]	Radial Position (in.)	Average BF_3 Counts per 100 Counts on Standard[1]
33.52	1116	12.77	3051
33.26	1083	11.77	3092
32.26	774	10.77	3201
31.24	554	9.77	3344
30.26	435	8.77	3427
29.26	412	7.77	3563
28.22	427	6.77	3653
27.26	479	5.77	3762
25.73	654	4.77	3791
24.26	914	4.07	3841
22.76	1258	2.77	3910
21.26	1789	1.77	3974
19.74	2570	0.77	3930
18.26	2785	0.27	4022
17.71	2754	-0.23	3944
16.77	2727	-0.73	4018
15.77	2752	1.23	4003
14.74	2818	-1.73	3969
13.76	2918		

[1] Count rate obtained using 1.5 x 10^4 standard count

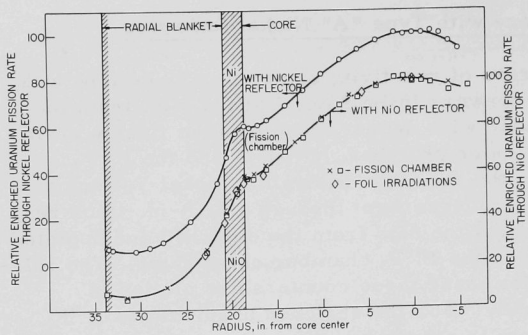

Fig. 69

Enriched Uranium Fission Rate Versus Radius at Midplane through Nickel and Nickel Oxide Reflectors

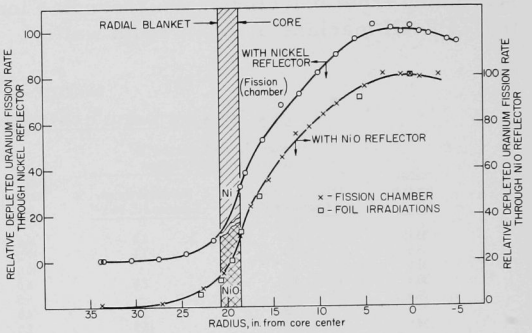

Fig. 70

Depleted Uranium Fission Rate Versus Radius at Midplane through Nickel and Nickel Oxide Reflectors

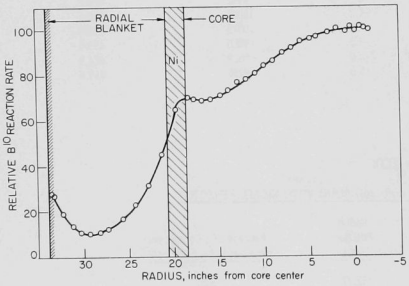

Fig. 71

Radial Traverse of $B^{10}F_3$ Counter at Midplane through Nickel Reflector

D. Radial Traverse at Midplane with Type "B" Nickel Oxide Reflectors

The radial traverses with the enriched uranium counter, J, and the depleted uranium counter, IC-24-1, were repeated after the replacement of Type "A" nickel with Type "B" nickel oxide composition in the radial reflector. For the enriched uranium traverse the equivalent nickel oxide

reflector thickness was 1.44 in., and for the depleted uranium traverse 1.49 in., with drawer 2-G-16 containing 2.18 in. reflector and the reflector drawers adjacent to 2-G-16 containing 1.47 in. Table XXX lists the count rates obtained for enriched and depleted uranium at the various radial positions. The enriched uranium fission rates are compared in Fig. 69 with those obtained through the nickel reflector. A decrease in U^{235} fission rate is observed near the nickel oxide reflector as compared with that near the nickel reflector. Figure 70 compares the fission rates of U^{238} in the two reflector cases. Also shown in Figs. 69 and 70 are U^{235} and U^{238} relative reaction rates with the Type "B," nickel oxide reflector obtained from foil irradiations (experiment described in Section XIII).

Table XXX

RADIAL FISSION RATE TRAVERSES AT CORE MIDPLANE WITH NiO REFLECTOR

Radial Position (in.)	Average Counts per 10^3 Standard Counts: Enriched Uranium, Counter J Trial 1[a]	Enriched Uranium, Counter J Trial 2[a]	Depleted Uranium, Counter IC-24-1[b]
33.75	1061	-	1.8
31.50	824	780	-
27.15	1402	1340	10.3
22.75	3651	3561	51.8
21.75	4359	-	-
20.50	5815	5678	96.2
19.30	7195	7162	-
18.50	7941	7698	204.4
17.50	8075	7973	282.6
16.20	8711	8454	-
15.50	-	-	352.5
14.00	9751	-	416.8
13.00	-	9818	-
12.50	-	-	480.7
12.00	10635	-	-
11.00	-	-	502.2
10.00	11812	11283	-
9.50	-	-	537.6
8.00	12601	-	563.8
7.00	-	12535	-
6.00	13088	-	-
5.00	-	-	614.4
4.00	13668	13166	-
3.00	-	-	647.4
2.00	14207	-	-
1.00	14336	13421	645.3
0.00	14081	13461	644.7
-1.00	14072	13574	637.4
-2.00	13900	-	-
-3.00	-	-	644.8
-4.00	13451	13228	-
-6.00	13704	-	-

(a)Rate obtained using standard count of 1×10^4.

(b)Rate obtained using standard count of 2×10^4.

XIII. FOIL IRRADIATIONS

Foils of enriched, natural, and depleted uranium were irradiated on four occasions to obtain fission and capture rates, and ratios for U^{235} and U^{238} under different circumstances. Two irradiations were made while the nickel reflector was in place, one with the nickel oxide reflector, and one during the beryllium-source experiment, the results of which have already been given in Table VII. Radiochemical techniques were used to obtain the fissions per foil by analysis for Mo^{97} and the captures by analysis for Np^{237}.

A. Foil Irradiations at Midplane with Nickel Reflector

The two irradiations while the reflector was of Type "A" nickel composition were done during experiments with fission chambers at the core center (see Section XIV). During these irradiations, the equivalent reflector thickness was about 1.75 in. In one run, the counters were in place at the front of 1- and 2-P-16, and enriched and natural uranium foils were irradiated in 1- and 2-P-16 at the front of the counters, in 1- and 2-P-14, in 1- and 2-P-8, and in 1- and 2-Z-16. Unusual results were obtained; the ratio $\sigma_f\ U^{238}/\sigma_f\ U^{235}$ in P-16 was lower than in P-14. To investigate this further, another irradiation was made in which the counters were removed and foils placed at the fronts of 1- and 2-P-16 (center of void counter space), near the core material in 1- and 2-P-16 (1 in. back from drawer front), and at the front of 1- and 2-P-14 (full core drawers). Again a lower $\sigma_f\ U^{238}/\sigma_f\ U^{235}$ was obtained from the foils in P-16. The results of the two irradiations are given in Table XXXI.

Table XXXI

FOIL IRRADIATIONS AT MIDPLANE WITH NICKEL REFLECTOR

	Position of Foils				
	Drawers	Radius (in.)	Arrangement	$\sigma_f\ U^{238}/\sigma_f\ U^{235}$	$\sigma_c\ U^{238}/\sigma_f\ U^{235}$
Trial No. 1	1 & 2-P-16	0.34	Fission chambers in first inch, foils at front	0.0291 ± 0.0021	0.103 ± 0.005
	1 & 2-P-14	4.37	Foils at front of full core drawers	0.0326 ± 0.0022	0.108 ± 0.005
	1 & 2-P-8	17.47	Foils at front of full core drawers	0.0226 ± 0.0015	0.118 ± 0.006
	1 & 2-Z-16	20.76	Foils at front, top of radial blanket drawer (outside edge of nickel reflector)	0.0112 ± 0.0008	0.112 ± 0.006
Trial No. 2	1 & 2-P-16	0.34	Void in first inch, foils at drawer front	0.0307 ± 0.0016	0.112 ± 0.005
	1 & 2-P-16	0.34	Void in first inch, foils 1 in. back from drawer front	0.0338 ± 0.0018	0.114 ± 0.005
	1 & 2-P-14	4.37	Foils at front of full core drawers	0.0347 ± 0.0018	0.114 ± 0.005

The variations in fission ratios according to where the foils were placed suggests that the anomalous results are due to fuel-proximity effects. Because of these effects, the best central ratios from these foil data therefore are those from the P-14 locations - giving an average $\sigma_f U^{238}/\sigma_f U^{235} = 0.0336$ and $\sigma_c U^{238}/\sigma_f U^{235} = 0.111$.

B. Foil Irradiations at Midplane with Nickel Oxide Reflector

Sets of enriched and natural uranium foils were irradiated at the reactor midplane when the radial reflector was of the Type "B" nickel oxide composition. At the time, the equivalent thickness of nickel oxide was 1.43 in. The foils were placed near the front of drawers at several radii, and the results are given in Table XXXII. Included in the table are the fissions and captures per gram in the foils. The relative U^{235} and U^{238} fission rates versus radii derived from these foils are graphed along with the counter traverse results in Figs. 69 and 70.

Table XXXII

FOIL IRRADIATIONS AT MIDPLANE WITH NICKEL OXIDE REFLECTOR

Foil Set No.	Average Foil Radius (in.)	Fissions/g Enriched Uranium[a] (x 10^9)	Fissions/g Natural Uranium (x 10^8)	Captures/g Natural Uranium (x 10^8)	$\sigma_f^{28}/\sigma_f^{25}$	$\sigma_c^{28}/\sigma_f^{25}$
1	1.00	15.0 ± 0.5	6.13 ± 0.18	17.8 ± 0.5	0.0316 ± 0.0013	0.112 ± 0.005
2	5.53	14.2 ± 0.4	5.60 ± 0.17	17.4 ± 0.5	0.0302 ± 0.0013	0.117 ± 0.005
3	16.40	8.80 ± 0.26	3.06 ± 0.09	11.6 ± 0.4	0.0258 ± 0.0011	0.124 ± 0.005
4	18.58	8.29 ± 0.25	2.25 ± 0.07	11.3 ± 0.3	0.0185 ± 0.0008	0.129 ± 0.005
5	19.54	7.82 ± 0.24	1.61 ± 0.06	10.2 ± 0.3	0.0123 ± 0.0006	0.123 ± 0.005
6	20.76	5.69 ± 0.17	1.01 ± 0.07	6.37 ± 0.19	0.0095 ± 0.0007	0.105 ± 0.004
7	22.93	3.60 ± 0.11	0.54 ± 0.05	4.17 ± 0.12	0.0069 ± 0.0007	0.109 ± 0.005

[a]Enriched uranium = 93.18 w/o U^{235}.

XIV. CENTRAL FISSION RATIOS

Ratios of fission cross sections of various fissionable isotopes were measured at the core center with absolute fission chambers of a basic design described by Kirn.(6) The original Kirn construction consisted of a thin plating of fissionable material on an inside face of a 2-in.-diameter x 1- in.-long steel-walled chamber with a parallel collector plate and a sealed-in argon-methane filling. Two sets of modified design counters were also used in which the fissile platings were on interchangeable foils and there was continuous gas flow; in one set, the chamber wall construction was the same as in the Kirn counters; in the other set, the walls were thin and the connector to the high-voltage cable was extended. These different types were used to study effects of chamber construction on the results. Figure 72 compares the three designs.

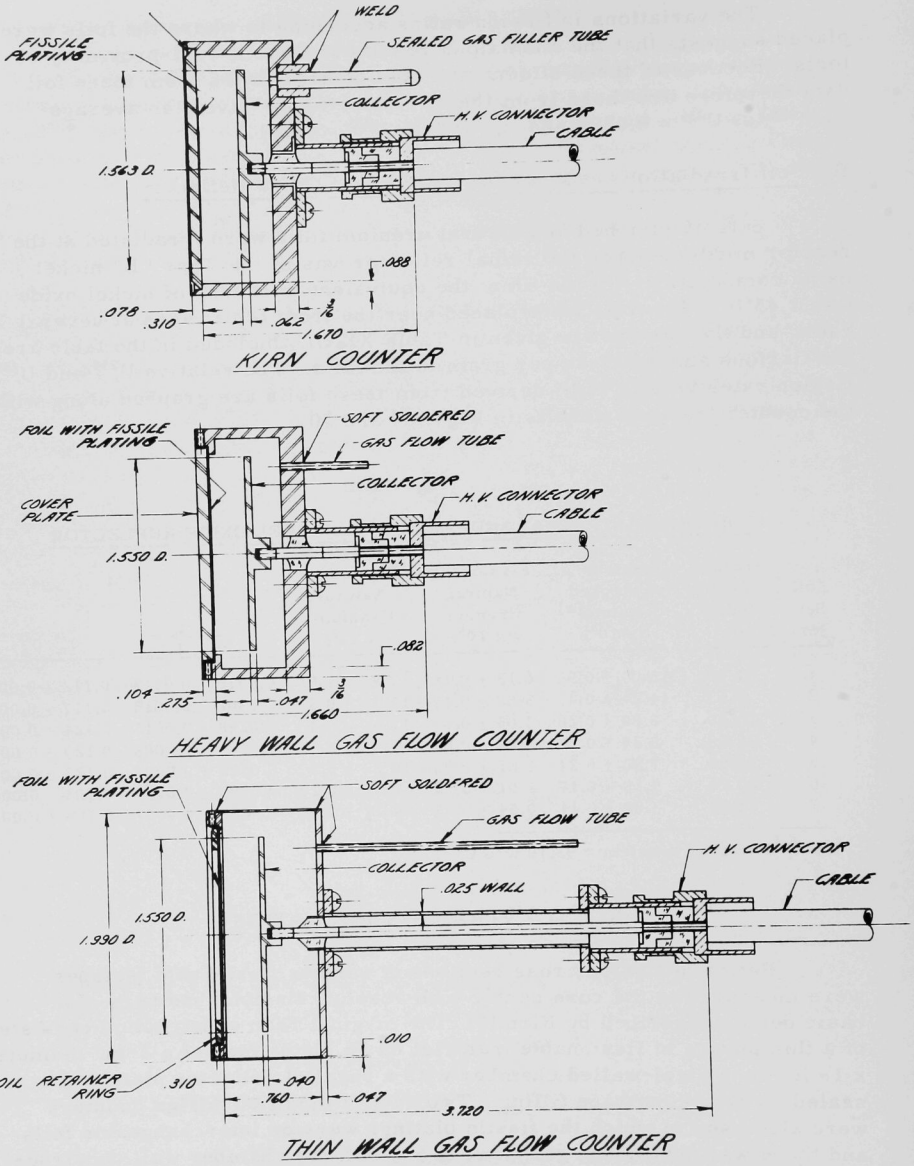

Fig. 72. Absolute Fission Chambers

Drawers 1- and 2-P-16 were modified to accommodate the chambers at the front and the connector cable along the drawer length. The $\frac{1}{8}$-in. fuel columns were replaced by two $\frac{1}{16}$-in. columns near the drawer edges. Pairs of the various counters were placed at the fronts of the drawers and ratios of count rates obtained. During these experiments, the radial reflector was of the Type "A" nickel composition and its equivalent thickness varied between 1.75 and 1.82 in.

Details of the experiments and their results are given in Table XXXIII. In the first five trials listed, ratios of count rates were measured between a U^{235} Kirn counter (enriched uranium plating) and Kirn counters with other principal isotopes. In trial f, the ratio of $\sigma_f U^{238}/\sigma_f U^{235}$ was measured using enriched and natural uranium foils in two heavy-walled gas-flow chambers, and the result agreed with the Kirn counter result (trial e) within experimental error. The foils were then used in thin-walled gas-flow counters and the result, given in trial g, showed a gain of 8 (±1)% in the $\sigma_f U^{238}/\sigma_f U^{235}$ ratio. Trial h was a repeat of trial g, in which a 1-in.-length of polyethylene-shielded cable was inserted behind each counter, and a decrease in U^{238}/U^{235} fission ratio was obtained (-1.6 ± 1%).

Table XXXIII

CENTRAL FISSION RATIO MEASUREMENTS WITH ABSOLUTE COUNTERS

Trial	Counter (Principal Isotope)	vs	Counter (Principal Isotope)	Fission Ratio(1)	Value(2)
a	Kirn #18 (U^{233})		Kirn #5 (U^{235})	$\sigma_f U^{233}/\sigma_f U^{235}$	1.409 ± 0.004
b	Kirn #11 (U^{234})		Kirn #5 (U^{235})	$\sigma_f U^{234}/\sigma_f U^{235}$	0.228 ± 0.002
c	Kirn #21 (Pu^{239})		Kirn #5 (U^{235})	$\sigma_f Pu^{239}/\sigma_f U^{235}$	1.086 ± 0.006
d	Kirn #12 (Pu^{240})		Kirn #5 (U^{235})	$\sigma_f Pu^{240}/\sigma_f U^{235}$	0.250 ± 0.004
e	Kirn #3 (U^{238})		Kirn #5 (U^{235})	$\sigma_f U^{238}/\sigma_f U^{235}$	0.0296 ± 0.0002
f	Heavy wall, gas flow with U^{238} foil		Heavy wall, gas flow with U^{235} foil	$\sigma_f U^{238}/\sigma_f U^{235}$	0.0290 ± 0.0003
g	Thin wall, gas flow with U^{238} foil		Thin wall, gas flow with U^{235} foil	$\sigma_f U^{238}/\sigma_f U^{235}$	0.0314 ± 0.0003
h	Thin wall, gas flow with U^{238} foil and CH_3		Thin wall, gas flow with U^{235} foil and CH_3	$\sigma_f U^{238}/\sigma_f U^{235}$	0.0309 ± 0.0002
i	Kirn #3 (U^{238})		Heavy wall, gas flow with U^{238} foil	$\frac{\sigma_f U^{238}\text{ (Kirn)}}{\sigma_f U^{238}\text{ (H.W.)}}$	0.972 ± 0.006
j	Kirn #5 (U^{235})		Heavy wall, gas flow with U^{235} foil	$\frac{\sigma_f U^{235}\text{ (Kirn)}}{\sigma_f U^{235}\text{ (H.W.)}}$	0.975 ± 0.004
k	Kirn #5 (U^{235})		Kirn #4 (U^{235})	$\frac{\sigma_f U^{235}\text{ (Kirn \#5)}}{\sigma_f U^{235}\text{ (Kirn \#4)}}$	0.998 ± 0.005

(1) Fissions from isotopes other than principal have been accounted for.

(2) Errors are observed variations of 4 or 5 count ratios.

In trial i, a Kirn U^{238} counter was compared with a heavy-walled gas-flow counter using a U^{238} foil, and trial j compared a Kirn U^{235} counter with a heavy-walled gas-flow counter with a U^{235} foil. Both trials i and j

indicated a difference in efficiency of about +2% between the Kirn chambers and the heavy-walled counters. In trial k, two Kirn U^{235} counters were compared and found to agree.

The data of these fission counter experiments indicate a sensitivity of the measurements to chamber construction and possibly to proximity at the connecting cable. These effects were predicted by calculations and were also observed in separate experiments by W. Davey and R. Curran[7] in Argonne's fast source reactor. It is seen that the thicker chamber walls give a lower U^{238}/U^{235} fission ratio, presumably due to inelastic-scattering effects. The effects, however, would not be serious for the non-threshold isotopes. The best values of fission ratios to be derived from the data are therefore as follows:

$$\sigma_f\, U^{238}/\sigma_f\, U^{235} = 0.0314 \pm 0.0003 \text{ (thin-walled, gas-flow chambers)}$$

$$\sigma_f\, U^{233}/\sigma_f\, U^{235} = 1.409 \pm 0.004 \text{ (Kirn counters)}$$

$$\sigma_f\, U^{234}/\sigma_f\, U^{235} = 0.228 \pm 0.002^{*} \text{ (Kirn counters)}$$

$$\sigma_f\, Pu^{239}/\sigma_f\, U^{235} = 1.086 \pm 0.006 \text{ (Kirn counters)}$$

$$\sigma_f\, Pu^{240}/\sigma_f\, U^{235} = 0.250 \pm 0.004^{*} \text{ (Kirn counters)}$$

*On the basis of the AFSR experiments,[7] a correction for wall-thickness effects of about +3% should be applied to the ratios for the threshold isotopes U^{234} and Pu^{240}.

REFERENCES

1. C. E. Branyan, Core A Critical Studies for the Enrico Fermi Atomic Power Plant, ANL-6629 (1962).

2. Enrico Fermi Atomic Power Plant, APDA-124 (1959).

3. B. C. Cerutti et al., ZPR-III, Argonne's Fast Critical Facility, Nuclear Science and Engr., 1, 126 (1956).

4. G. S. Brunson et al., Measuring the Prompt Period of a Reactor, Nucleonics 15 (11), 32 (1957).

5. Reactor Development Program, Progress Report April 1961, ANL-6301 p. 61 (1961).

6. F. S. Kirn, An Absolute Fission Counter, American Nuclear Society, 2nd Winter Meeting (1957).

7. W. G. Davey and R. N. Curran, An Experimental Investigation of Some Sources of Error in the Measurement of Absolute Fission Ratios in Fast Reactors, ANL-6468 (Nov 1961).

8. C. B. Mills, Neutron Cross Sections for Fast and Intermediate Nuclear Reactors, LAMS-2255 (Jan 1959).

9. G. R. Keepin, T. F. Wimett, and R. K. Zeigler, Delayed Neutrons from Fissionable Isotopes of Uranium, Plutonium and Thorium, LA-2118 (1957).

10. Topolnicki, APDA Memo RSA 61-229 (Internal Memo).

APPENDIX A

ZPR-III, Assembly 35 Specifications

ZPR Matrix Tubes	2.184 x 2.175 x 33.5 in.; cross-sectional area: 4.75 in.^{2}
Front Drawers	2.06 x 2.03 x 21.25 in.
Back Drawers	2.06 x 2.03 x 11.25 in.
Control Drawers	2.06 x 2.03 x 32.5 in.

COMPOSITIONS OF CORE DRAWER

Volume of Core Section: 1.4034 liters per drawer

	Weights in Core Section per Drawer, gm					Total Drawers	
Drawer	93.2% Enriched Uranium	Stainless Steel*	Iron	Oxygen	Sodium	666.7-liter Core	599.3-liter Core**
Type 1	1310.9	4493.7	498.7	198.8	447.6	53	44
Type 2	1310.9	5436.1	498.7	198.8	335.7	56	52
Type 3	1310.9	4493.7	498.7	198.8	447.6	59	54
Type 4	1310.9	5053.4	249.3	99.4	447.6	61	49
Type 5	0	6186.7	0	0	447.6	60	52
Type 6	1310.9	5448.5	498.7	198.8	335.7	62	50
Type 7	1310.9	4493.7	498.7	198.8	447.6	58	54
Type 8	1310.9	5045.7	249.3	99.4	447.6	56	52
Safety Rod No. 2 and 7	1310.9	5629.2	498.7	198.8	334.8	2	2
Safety Rod No. 3, 8, and 9	1310.9	5240.2	249.3	99.4	446.4	3	3
Safety Rod No. 4, 5, and 6	1310.9	4682.0	498.7	198.8	446.4	3	3
Control Rod No. 1 and 10	1310.9	4682.0	498.7	198.8	446.4	2	2

*Includes the stainless steel in the sodium cans, matrix, and drawers.

**Edge drawers not included.

$$\text{Core L/D} = \frac{36.06}{35.94} = 1.003$$

APPENDIX B

Derivation of Inhour Curve

A spherical model of the Core B critical assembly, in which the shape factor was taken to be 1.088, was used in an AIM-6 calculation to get the space and energy distributions of the real and adjoint fluxes. This code solves the multigroup one-dimensional diffusion equations with the Los Alamos 18-group set of cross sections[8] modified for the low-energy groups of stainless steel.

Taking these fluxes and the delayed-neutron data of Keepin[9] as input, the DENEF code, written by APDA,[10] was used to calculate the effective delayed-neutron fraction β^i_{eff} for each delayed-neutron group, and the neutron lifetime ℓ. These quantities are defined as

$$\beta^i_{eff} = \frac{\text{importance of delayed neutrons}}{\text{the rate of production of importance for the } i^{th} \text{ delayed group}}$$

$$\ell = \frac{\text{total importance of all neutrons in the reactor}}{\text{the rate of production of importance}} .$$

These quantities are used in the following inhour relation:

$$\rho(T) = \frac{(\ell/T) + \sum_{i=1}^{6} \frac{\beta^i_{eff}}{1 + \lambda_i T}}{1 + (\ell/T)} ,$$

where

ρ = reactivity $\Delta k/k$

λ_i = decay constant for the i^{th} group

T = reactor period, sec.

The relation is plotted in Fig. 73. For low amounts of reactivity the relation between inhours and dollars is given by

$$\frac{1}{\rho} \sum_{i=1}^{6} \frac{\beta^i_{eff}}{\lambda_i} = \frac{3600}{\text{inhours}} .$$

The above calculations were performed for the nickel-reflected 600-liter core assembly and gave the following values:

Neutron lifetime $\ell = 3.97 \times 10^{-7}$ sec

Total effective delayed-neutron fraction $\beta_{eff} = \sum_{i=1}^{6} \beta^{i}_{eff}$

$= 6.65 \times 10^{-3}$

288 inhours = 1 dollar

The control-rod calibration given in Fig. 25 was obtained from the above inhour relation and period measurements in the reactor. For the calibration in the 666.7-liter core (see Fig. 21) without nickel reflector, the inhour curve was recalculated but found to be insignificantly different to that for the nickel-reflected core.

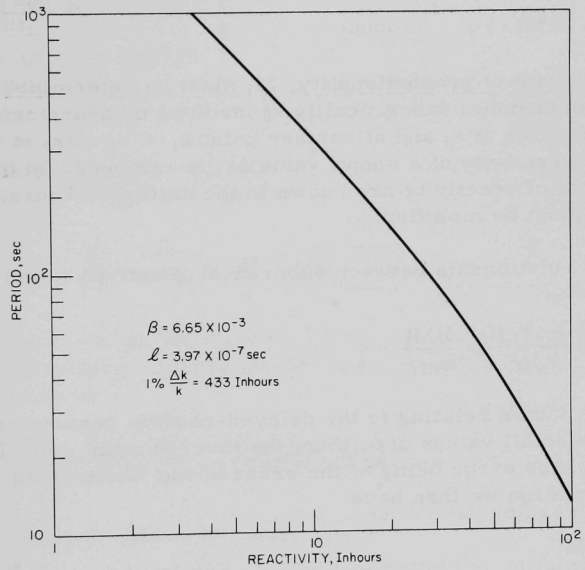

Fig. 73. Inhour Curve for Assembly 35 with 599-liter Core and Type "A" Nickel Reflector

APPENDIX C

Measurement of Reactor Subcriticality with BF_3 Neutron Counters in ZPR-III

For values of reactor k_{eff} less than one, steady-state multiplication of source neutrons as detected by BF_3 chamber count rates varies as

$$\text{Count Rate } R = A \frac{S}{1 - k_{eff}} \quad , \tag{1}$$

where S is the source strength and A is some constant depending on the position and characteristics of the chamber. Although S decreases by about $\frac{1}{2}$% per day (if a polonium-beryllium source is used), during a few hours of run S can be considered constant. If we call $I = R^{-1}$ (inverse count rate), the subcriticality varies as

$$1 - k = MI \quad , \tag{2}$$

where the constant of proportionality, M, must be determined. The determination of an unknown subcriticality k_0 involves measurement of the inverse count rates at k_0 and at another point $k_1 = k_0 - \Delta k_1$ at which an increment of reactivity of a known value Δk_1 is removed. In the case where the increments of reactivity are known in the units of inhours, the above relationship must be modified.

If the relationship between subcritical reactivity ρ and k_{eff} is used, Eq. (2) becomes

$$\rho = B \frac{1 - k_{eff}}{k_{eff}} = \frac{BMI}{k_{eff}} \quad , \tag{3}$$

where B is a factor relating to the delayed-neutron parameters of the reactor. For small values of ρ, then, the inverse count rate I is proportional to ρ, the error being of the order of the %k involved. For a first approximation we then have

$$\rho \approx BMI \quad . \tag{4}$$

The factor BM is obtained from the difference of values of I for different subcritical points of known separation $\Delta\rho$. Thus, from a value I_0 found at an unknown ρ_0 and a value I_i found at $\rho_i = \rho_0 + \Delta\rho_i$, where $\Delta\rho_i$ is known, ρ_0 is determined by

$$\rho_0 \approx \frac{I_0 \Delta\rho_i}{I_i - I_0} \tag{5}$$

As mentioned, the error in Eq. (5) is about (1-k)/k x 100%. To correct for this error, we develop a method as follows:

From Eq. (3), we find k and expand:

$$k = \frac{B}{\rho + B} = \frac{1}{1 + \rho/B} = 1 - \rho/B + \rho^2/B^2 - \rho^3/B^3 \ldots \quad (6)$$

Eq. (2) becomes

$$MI = (\rho/B) - (\rho^2/B^2) + (\rho^3/B^3) \ldots \quad (7)$$

For 1 - k or ρ/B of order 0.05 or less, $\rho^3/B^3 \leq 0.0025\ \rho/B$ and will be ignored. Thus, for subcritical points ρ_0 and $\rho_i = \rho_0 + \Delta\rho_i$,

$$\left.\begin{aligned} MI_0 &= (\rho_0/B) - (\rho_0^2/B^2) \\ MI_i &= (\rho_i/B) - (\rho_i^2/B^2) \end{aligned}\right\} \quad (8)$$

and

$$M(I_i - I_0) = \frac{\rho_i - \rho_0}{B} \quad \frac{\rho_i^2 - \rho_0^2}{B^2}$$

$$= \frac{\Delta\rho_i}{B} - \frac{\Delta\rho_i}{B^2}(2\rho_0 + \Delta\rho_i) \quad . \quad (9)$$

Since the second term on the right in Eq. (9) is a correction to the first of the order of 5% or less, we may use the approximate value of ρ_0 from Eq. (5) and arrive at

$$M(I_i - I_0) = \frac{\Delta\rho_i}{B} - \frac{\Delta\rho_i}{B^2}\left(\frac{2I_0\Delta\rho_i}{I_i - I_0} + \Delta\rho_i\right) \quad , \quad (10)$$

which gives finally the proportionality factor

$$M = \frac{\Delta\rho_i}{B(I_i - I_0)}\left[1 - \frac{\Delta\rho_i}{B(I_i - I_0)}(I_i + I_0)\right] \quad . \quad (11)$$

Then, M of Eq. (11) is used to find the initial subcriticality ρ_0 with the exact expression

$$\rho_0 = \frac{BMI_0}{1 - MI_0} \quad . \quad (12)$$

In the subcritical runs, count rates are obtained with all rods in (ρ_0) and at two or more other points (ρ_i). For each set ρ_0 - ρ_i a value of M is found from Eq. (11) and then ρ_0 found with Eq. (12) by use of the average value of M.

An estimation of the difference between deriving ρ_0 by this method and by using the approximate Eq. (5) is obtained by expanding (12) and using (11) to give

$$\rho_0 = \frac{\Delta\rho_i I_0}{I_i - I_0}\left[1 - \frac{\Delta\rho_i I_i}{B(I_i - I_0)} + \frac{\Delta\rho_i^2 I_i}{B^2(I_i - I_0)} \cdots\right] .$$

Thus, the error in (5) is about equal to $\Delta\rho_i I_i / B(I_i - I_0)$. Generally, $\Delta\rho_i$ is at the most 200 inhours, and for $I_i = 1.5\ I_0$ with $B = 4.3 \times 10^4$ the error would be around 1.4%.

ACKNOWLEDGEMENTS

This report presents the results of an experimental program to which many people contributed their time and efforts. The critical studies for Fermi Core B were carried out with Argonne National Laboratory's Zero Power Reactor III (ZPR-III) under the direction of F. W. Thalgott. Objectives of the initial program were established by J. B. Nimms of Atomic Power Development Associates in conjunction with ANL personnel. During the conduct of the experiments, evaluations of results and revisions of the program were made by R. Beaudry, R. Mueller, and E. Page of APDA. Personnel of the Idaho Division of ANL assisting with the planning, coordination and supervision of the ZPR-III experiments were J. K. Long, J. M. Gasidlo, R. L. McVean, R. J. Huber and W. P. Keeney. Acknowledgements are due also to R. J. Armani for radiochemical foil analysis, E. Slansky for computational assistance, W. P. Rosenthal for editing of this report, and to the ZPR technicians.

The authors are indebted to J. K. Long and F. W. Thalgott for their guidance in the experimental program and their reviews and comments on this report.